4

STRUCTURE DETERMINATION BY DIFFRACTION AND SCATTERING

4.0 INTRODUCTION

This chapter contains articles on six techniques that provide structural information on surfaces, interfaces, and thin films. They use X rays (X-ray diffraction, XRD, and Extended X-ray Absorption Fine-Structure, EXAFS), electrons (Low-Energy Electron Diffraction, LEED, and Reflection High-Energy Electron Diffraction, RHEED), or X rays in and electrons out (Surface Extended X-ray Absorption Fine Structure, SEXAFS, and X-ray Photoelectron Diffraction, XPD). In their "usual" form, XRD and EXAFS are bulk methods, since X rays probe many microns deep, whereas the other techniques are surface sensitive. There are, however, ways to make XRD and EXAFS much more surface sensitive. For EXAFS this converts the technique into SEXAFS, which can have submonolayer sensitivity.

The techniques can be broadly classified into two groups: those which directly identify the atomic species present and then provide structural information about the identified species from diffraction or scattering effects (EXAFS, SEXAFS, and XPD); and those which are purely diffraction-based and do not directly identify the atoms involved, but give long-range order information on atomic positions from

diffraction patterns (XRD, LEED, and RHEED). The latter group is only concerned with crystalline material and, for individual crystalline phases present, average unit cell dimensions, symmetries, and orientations are obtained directly from the diffraction patterns. Deviations from the average, i.e., defects of some sort, show up as a broadening of diffraction peaks, or, if they are periodic, as splittings of peaks.

XRD is the most widely used technique for general crystalline material characterization. Owing to the huge data bank available covering practically every phase of every known material (powder diffraction patterns), it is routinely possible to identify phases in polycrystalline bulk material and to determine their relative amounts from diffraction peak intensities. Phase identification for polycrystalline thin films, using standard equipment and diffraction geometries, is also possible down to thicknesses of 100 Å. For completely random polycrystalline thin films relative amounts are also easily determined. Once preferred orientations occur (texturing) this gets more difficult, requiring the collection of much more data or the introduction of more sophisticated equipment with different diffraction geometries so that the orientations can be "seen" effectively. These diffraction geometries include Grazing Incidence XRD (GIXRD), in which case the X-ray probing depth is greatly reduced. This has the effect of greatly improving surface sensitivity and allowing a depth profiling mode (50 Å to microns) by varying the incidence angle. When coupled to a synchrotron radiation X-ray source (to produce an intense, parallel X-ray beam) monolayer sensitivity can be achieved by GIXRD. GIXRD can therefore be used for the extreme situation of surface structure, or epitaxial relationships at the interfaces of films, where atomic positions can be determined to an accuracy of 0.001 Å in favorable cases.

Besides phase identification XRD is also widely used for strain and particle size determination in thin films. Both produce peak broadenings, but they are distinguishable. Compared to TEM, XRD has poor area resolution capability, although by using synchrotron radiation beam diameters of a few μm can be obtained. Defect topography in epitaxial films can be determined at this resolution.

Since LEED and RHEED use electron, instead of X ray, diffraction, the probing depths are short and surface crystallographic information is provided. Vacuum is also required. LEED uses normal incidence, with electron energies between 10 and 1000 eV, whereas RHEED (5–50 keV) uses grazing incidence and detection. The grazing geometry restricts RHEED information to the top few atomic layers, even though it is intrinsically less surface sensitive than the lower energy LEED. In both cases diffraction comes from two-dimensional rows of atoms, compared to the three-dimensional planes of atoms in XRD. In LEED the diffraction pattern (electron intensity "spots" projected back onto a phosphor screen; cf., an X-ray back-reflection Laue diffraction photograph) directly reveals the size and shape of the unit cell of the outermost, ordered atomic layer of single crystal material. To establish the locations of the atoms within the unit cell and the separation of the surface

plane from the bulk requires detailed measurements of the diffraction peak intensities versus the incident electron energy (wavelength), plus a comparison to a complex theoretical treatment of the electron scattering process in the material. Because of this only relatively few laboratories use LEED this way to determine the structures of clean, terminated bulk surfaces (which are often different from the bulk) and ordered adsorbed overlayers. The major use is to qualitatively check that single crystal surfaces are "well-ordered" and to determine the unit cell symmetries and dimensions of adsorbed overlayers. In analogy to the three-dimensional situation with XRD, disorder in the surface plane broadens LEED diffraction spots, and, if periodic, splits them. Information on finite island sizes (cf., particle size by XRD), strain, step densities, etc., can be obtained from detailed studies of the peak line shapes. Owing to its grazing angle geometry it is more complex, in general, to extract unit cell parameters from RHEED. If, however, the incident beam is aligned along a major surface crystallographic direction, this can be achieved fairly simply. Again, surface disorder translates to diffraction spot broadening. In practice RHEED is used primarily to monitor *in situ* the nucleation and growth of epitaxial films (e.g., MBE). The grazing geometry leaves the surface very "open" for the deposition process. In addition it makes RHEED very sensitive to surface roughness effects, such as island formation, since the reflected beam is actually transmitted through island "asperities," giving rise to new diffraction features. In standard form neither LEED nor RHEED have much spatial resolution, beam spot sizes being a fraction of a mm. Microscopic modes exist, however, using electron beam columns. They are Low-Energy Electron Microscopy, LEEM, and Scanning Reflection Electron Microscopy, SREM. Neither technique is discussed here, since they are too specialized.

In EXAFS a tunable source of X rays (supplied by a synchrotron facility) is used to scan energies from below to above the Binding Energy, BE, of electron core levels for any atom present. An increase in absorption associated with excitation of that electron occurs at the BE. Detection of such absorption "edge jumps" (usually measured using transmission through many thousands of angstroms of material) directly identifies the atoms present. Above the absorption edge weak periodic oscillations in the absorption strength occur due to interferences between the outgoing photoelectron wave from the absorbing atom and backscattering of this wave from neighboring atoms. The oscillations thus contain local radial distribution information (within ~5 Å of the absorbing atom). The frequency (or frequencies) of the oscillations relate to the distance of the surrounding atomic shell (or shells); the amplitudes relate to the number and types of surrounding atoms. If multiple sites of the specific element concerned are present a superimposition of oscillation frequencies is obtained that can be difficult to analyze, but for single site situations accuracies to ~ 0.03 Å in bond length can be achieved using model compounds of known structure. Since local order is probed, the material need not be crystalline. High-Z elements are more easily studied than low-Z elements, because the signal

strengths are higher and because, in general, the regions above their higher energy core level BEs are clear of other interfering absorption features over a large energy range. In bulk materials heavy elements can be detected and studied down to around 100 ppm. Also, for X-ray energies above ~5 keV samples can be studied under ambient pressures instead of in vacuum. The technique is widely used for bulk catalysts and in biological materials.

If the emitted electron intensity resulting from the core-level excitation process is used to detect the X-ray absorption process (in reflection), the bulk EXAFS method is turned into the surface-sensitive SEXAFS technique, where the depths probed are only a few atomic layers. Surface structures (absorption sites, bond lengths) for atoms absorbed on single crystal surfaces have been determined this way. The advantage compare to LEED is that the information is element specific, and long-range order of the adsorbate is not required. Accurate information is only obtainable, however, when the atom occupies a single unique site. Often C, O, N, S, etc., are studied. These light elements have core levels in the low-energy "soft X-ray" region so that vacuum techniques are required. For monolayer surface studies this is always true, anyway. It is also possible to use X-ray fluorescence as a detection scheme, instead of electrons. In this case the probing depth is extended to many hundreds of angstroms for the light elements, and deeper for the heavy elements.

For molecules adsorbed on surfaces strong features often appear in the spectrum at or very near the absorption edge-jumps (termed Near Edge X-ray Absorption Fine Structure, NEXAFS.) These are excitations from the core level to specific unoccupied molecular orbitals characteristic of the internal bonding of the molecule. From the response of the strength of these features to changes in the polarization of the X-ray beam, the orientation of the molecule with respect to the surface can be determined. Shifts in position of the features can also be related to internal bond length changes to an accuracy of about 0.05 Å. NEXAFS features are also sensitive to such things as oxidation states and chemical coordination. They can be used, for example, to identify different chemical groupings at polymer surfaces, or to identify reaction products at metal–semiconductor interfaces.

XPD is an extension of XPS (Chapter 5). In XPS X rays of a fixed wavelength, hν, eject core-level electrons from atoms in the sample. The kinetic energy, KE of these photoelectrons is measured, thereby allowing a determination of the core-level BEs (hν–KE), which provides an atomic identification and chemical state information in some cases. In XPD the angular distributions of these atom specific photoelectrons are measured for materials possessing long range order (usually single crystal surfaces, or for adsorption or reaction at these surfaces). The angular distributions are generated by diffraction of the photoelectron emitted from the target atom by its neighboring atoms. At the photoelectron energies involved the electron–atom scattering events peak in the forward direction, leading to the simple result that intensity maxima occur along atomic rows. Direct crystallographic infor-

mation about the near surroundings of the target atom is thus obtained. By comparing detailed calculations of the scattering processes for assumed models to the data, atom spacings can be obtained to an accuracy of ~ 0.05 Å. The probing depth is the same as for XPS; a few atomic layers. Strain, alloying, island formation, or interdiffusion during epitaxial growth is observable because the angular distributions are sensitive to atoms moving to "off-site" positions. XPD has been used as a simple diagnostic tool for distinguishing growth modes in well-ordered systems.

Auger Electron Diffraction, AED, is an exact analogy to XPD, providing basically the same information. Instead of measuring the angular distribution of the ejected photoelectrons one uses the Auger electrons (Chapter 5).

4.1 XRD

X-Ray Diffraction

MICHAEL F. TONEY

Contents

Introduction

X-ray Diffraction (XRD) is a powerful technique used to uniquely identify the crystalline phases present in materials and to measure the structural properties (strain state, grain size, epitaxy, phase composition, preferred orientation, and defect structure) of these phases. XRD is also used to determine the thickness of thin films and multilayers, and atomic arrangements in amorphous materials (including polymers) and at interfaces.

XRD offers unparalleled accuracy in the measurement of atomic spacings and is the technique of choice for determining strain states in thin films. XRD is noncontact and nondestructive, which makes it ideal for in situ studies. The intensities measured with XRD can provide quantitative, accurate information on the atomic arrangements at interfaces (e.g., in multilayers). Materials composed of any element can be successfully studied with XRD, but XRD is most sensitive to high-Z elements, since the diffracted intensity from these is much larger than from low-Z elements. As a consequence, the sensitivity of XRD depends on the material of interest. With lab-based equipment, surface sensitivities down to a thickness of ~50 Å are achievable, but synchrotron radiation (because of its higher intensity)

allows the characterization of much thinner films, and for many materials, monatomic layers can be analyzed. While the structure as a function of depth is not normally measured in XRD, this is possible using specialized methods.

Alternatives to XRD include transmission electron microscopy (TEM) and diffraction, Low-Energy and Reflection High-Energy Electron Diffraction (LEED and RHEED), extended X-ray Absorption Fine Structure (EXAFS), and neutron diffraction. LEED and RHEED are limited to surfaces and do not probe the bulk of thin films. The elemental sensitivity in neutron diffraction is quite different from XRD, but neutron sources are much weaker than X-ray sources. Neutrons are, however, sensitive to magnetic moments. If adequately large specimens are available, neutron diffraction is a good alternative for low-Z materials and for materials where the magnetic structure is of interest.

While XRD is nondestructive and can be used in most environments, TEM and electron diffraction are destructive techniques (due to specimen preparation methods) and require high vacuum. One of the disadvantages of XRD, compared to electron diffraction, is the low intensity of diffracted X rays, particularly for low-Z materials. Typical intensities for electron diffraction are $\sim 10^8$ times larger than for XRD. Because of small diffracted intensities, thin-film XRD generally requires large specimens (~0.5 cm) and the information acquired is an average over a large area. Usually, XRD does not provide spatial resolution, but for special applications, resolution of greater than ~10 μm can be obtained with a microfocus source and a suitably thick film ~1μm). The use of intense synchrotron X-ray radiation mitigates these two disadvantages somewhat; however, the XRD analysis of thin films with synchrotron radiation is not routine (because of the limited accessibility of synchrotron sources).

Thin-film XRD is important in many technological applications, because of its abilities to accurately determine strains and to uniquely identify the presence and composition of phases. In semiconductor and optical materials applications, XRD is used to measure the strain state, orientation, and defects in epitaxial thin films, which affect the film's electronic and optical properties. For magnetic thin films, it is used to identify phases and to determine preferred orientations, since these can determine magnetic properties. In metallurgical applications, it is used to determine strains in surface layers and thin films, which influence their mechanical properties. For packaging materials, XRD can be used to investigate diffusion and phase formation at interfaces

Basic Principles

This section briefly discusses the fundamental principles of XRD; the reader is referred to the works by Warren, Cullity, and Schwartz and Cohen for more detail.[1–3] Figure 1 shows the basic features of an XRD experiment, where the diffraction angle 2θ is the angle between the incident and diffracted X rays. In a typical

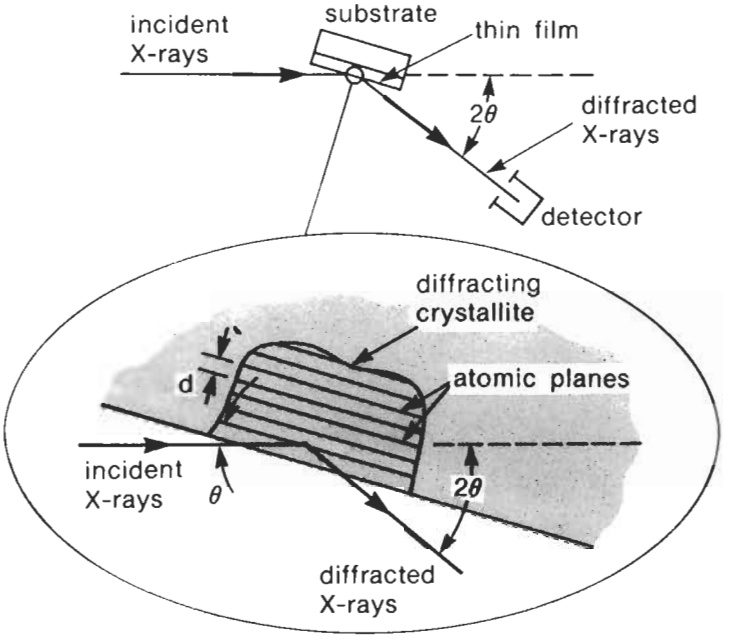

Figure 1 **Basic features of a typical XRD experiment.**

experiment, the diffracted intensity is measured as a function of 2θ and the orientation of the specimen, which yields the diffraction pattern. The X-ray wavelength λ is typically 0.7–2 Å, which corresponds to X-ray energies (E = 12.4 keV/λ) of 6 – 17 keV.

The Directions of Diffracted X Rays

Before considering the conditions for XRD, we will briefly review some important properties of crystalline materials. Crystals consist of planes of atoms that are spaced a distance d apart (Figures 1 and 2), but can be resolved into many atomic planes, each with a different d-spacing. To distinguish between these, we introduce a coordinate system for the crystal whose unit vectors a, b, and c are the edges of the unit cell (Figure 2b). For the familiar cubic crystal, these form an orthogonal system. Any atomic plane can now be uniquely distinguished by its Miller indices. These are the three reciprocal intercepts of the plane with the a-, b-, and c-axes and are reduced to the smallest integers having the same ratio. Thus, an (hkl) plane intercepts the crystallographic axes at a/h, b/k, and c/l; examples are shown in Figure 2. The d-spacing between (hkl) planes is denoted d_{hkl}, and for cubic crystals, it is

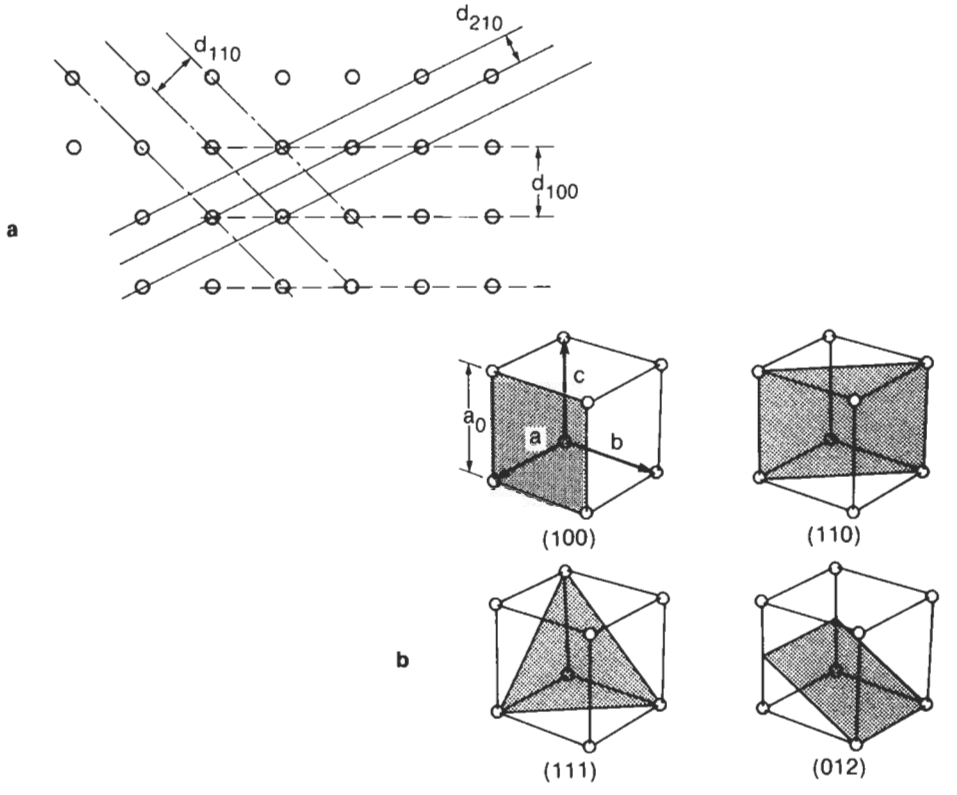

Figure 2 **Several atomic planes and their d-spacings in a simple cubic (sc) crystal (a); and Miller indices of atomic planes in an sc crystal (b). As an example consider the (012) plane. This intercepts the a-, b-, and c-axes at ∞, 1, and 1/2, respectively, and thus, h = 1/∞ = 0, k = 1/1 = 1, and l = 1/(1/2) = 2.**

$$d_{hkl} = \frac{a_0}{\sqrt{h^2 + k^2 + l^2}} \tag{1}$$

where a_0 is the lattice constant of the crystal (see Figure 2).

When there is constructive interference from X rays scattered by the atomic planes in a crystal, a diffraction peak is observed. The condition for constructive interference from planes with spacing d_{hkl} is given by Bragg's law:

$$\lambda = 2d_{hkl} \sin\theta_{hkl} \tag{2}$$

where θ_{hkl} is the angle between the atomic planes and the incident (and diffracted) X-ray beam (Figure 1). For diffraction to be observed, the detector must be positioned so the diffraction angle is $2\theta_{hkl}$, and the crystal must be oriented so that the normal to the diffracting plane is coplanar with the incident and diffracted

X rays and so that the angle between the diffracting plane and the incident X rays is equal to the Bragg angle θ_{hkl}. For a single crystal or epitaxial thin film, there is only one specimen orientation for each (hkl) plane where these diffraction conditions are satisfied.

Thin films, on the other hand, can consist of many grains or crystallites (small crystalline regions) having a distribution of orientations. If this distribution is completely random, then diffraction occurs from any crystallite that happens to have the proper orientation to satisfy the diffraction conditions. The diffracted X rays emerge as cones about the incident beam with an opening angle of $2\theta_{hkl}$, creating a "powder" diffraction pattern. Thin films are frequently in a class of materials intermediate between single crystals and powders and have fiber texture. That is, all the crystallites in the film have the same atomic planes parallel to the substrate surface, but are otherwise randomly distributed. Face-centered cubic (fcc) films often grow with (111) fiber texture: The (111) planes are parallel to the substrate plane and planes perpendicular to this—e.g., (220)—are necessarily perpendicular to the substrate but otherwise randomly distributed. The resulting diffraction pattern consists of rings about the film normal or (111) axis. Thin films may not have complete fiber texture, but may possess a preferred orientation, where most, but not all, of the crystallites have the same atomic planes parallel to the substrate. For example, while most of the fcc film might have (111) texture, a few of the crystallites might have their (200) planes parallel to the substrate.

As we have seen, the orientation of crystallites in a thin film can vary from epitaxial (or single crystalline), to complete fiber texture, to preferred orientation (incomplete fiber texture), to randomly distributed (or powder). The degree of orientation not only influences the thin-film properties but also has important consequences on the method of measurement and on the difficulty of identifying the phases present in films having multiple phases.

Intensities of Diffracted X Rays

Before considering diffracted intensities, we first must consider X-ray absorption, since this affects intensities. All materials absorb X rays. Thus, an X-ray beam is attenuated as it traverses matter. The transmitted intensity decays exponentially with the distance traveled through the specimen and the linear absorption coefficient μ describes this decrease. The absorption length ($1/e$ decay length) is $1/\mu$, and at $\lambda = 1.54$ Å, typical values are 1 mm, 66 μm, and 4 μm for carbon, silicon, and iron, respectively. Except near an absorption edge,[1–3] μ increases with increasing atomic number and increasing wavelength.

Neglecting unimportant geometric factors,[1–3] the integrated X-ray intensity diffracted from a thin film is

$$I_{hkl} \propto |F_{hkl}|^{-2M} V \tag{3}$$

Here F_{hkl} is the structure factor for the (hkl) diffraction peak and is related to the atomic arrangements in the material. Specifically, F_{hkl} is the Fourier transform of the positions of the atoms in one unit cell. Each atom is weighted by its form factor, which is equal to its atomic number Z for small 2θ, but which decreases as 2θ increases. Thus, XRD is more sensitive to high-Z materials, and for low-Z materials, neutron or electron diffraction may be more suitable. The factor e^{-2M} (called the Debye-Waller factor) accounts for the reduction in intensity due to the disorder in the crystal, and the diffracting volume V depends on μ and on the film thickness. For epitaxial thin films and films with preferred orientations, the integrated intensity depends on the orientation of the specimen.

Dynamical X-Ray Diffraction

In the concepts developed above, we have used the kinematic approximation, which is valid for weak diffraction intensities arising from "imperfect" crystals. For perfect crystals (available thanks to the semiconductor industry), the diffraction intensities are large, and this approximation becomes inadequate. Thus, the dynamical theory must be used. In perfect crystals the incident X rays undergo multiple reflections from atomic planes and the dynamical theory accounts for the interference between these reflections. The attenuation in the crystal is no longer given by absorption (e.g., μ) but is determined by the way in which the multiple reflections interfere. When the diffraction conditions are satisfied, the diffracted intensity from perfect crystals is essentially the same as the incident intensity. The diffraction peak widths depend on $2\theta_{hkl}$ and F_{hkl} and are extremely small (less than ~0.001–0.005°).

Experimental Methods for Thin Film Characterization by XRD

Because the diffracting power of thin films is small, the instrumentation and techniques for thin-film XRD are designed to maximize diffracted intensities and to minimize background. There are basically two classes of measurement techniques. The first, and oldest, uses photographic film; these methods provide fast, preliminary information and yield two-dimensional data. However, progress in computers and high-power X-ray generators has lead to the widespread use of diffractometers, where the diffracted X rays are detected with photon counters. Compared to photographic methods, counters provide more accurate, quantitative data and have superior signal-to-noise ratios. Furthermore, diffractometers are easily automated and provide better angular resolution. Recently, there has been increasing use of position-sensitive detectors,[2, 3] which use parallel detection to scan a range in 2θ.

X-Ray Diffractometer Methods

The Bragg-Brentano geometry [2–4] is used widely for preferentially and randomly oriented polycrystalline films. In this geometry (Figure 3a), slits collimate the inci-

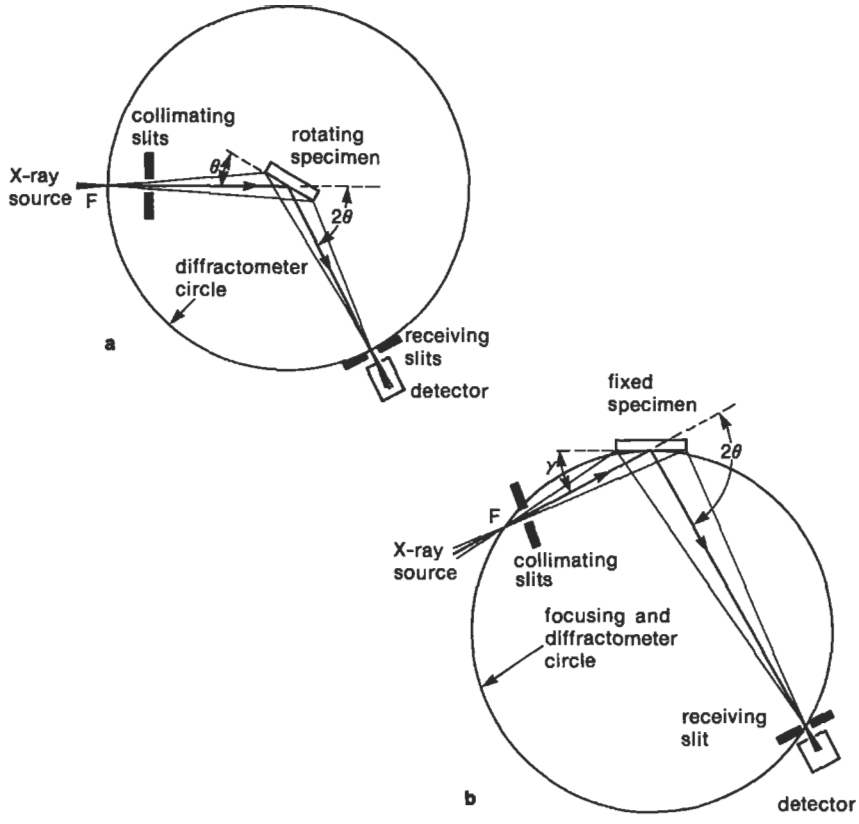

Figure 3 **Bragg-Brentano diffractometer (a); and Seemann-Bohlin diffractometer (b). The point F is either the focal point on an X-ray tube or the focal point of a focusing monochromator.**

dent X rays, which impinge on the specimen at an angle θ. After passing through receiving slits, the diffracted X rays are detected. The specimen is rotated at one-half the angular velocity of the detector. Since the incident and diffracted X rays make the same angle to the specimen surface, structural information is obtained only about (hkl) planes parallel to this surface. When the receiving slits, the specimen, and the focal point F lie on a circle, the diffracted X rays are approximately focused on the receiving slits (parafocusing), which considerably improves the sensitivity.

For the Seemann-Bohlin geometry (Figure 3b) the incident X rays impinge on a fixed specimen at a small angle $\gamma \sim 5$–$10°$ and the diffracted X rays are recorded by a detector that moves along the focusing circle.[2–4] This method provides good sensitivity for thin films, due to parafocusing and the large diffracting volume, which results from γ being small and the X-ray path length in the film being large (propor-

tional to $1/\sin\gamma$). Because γ is fixed, the angle between the incident X rays and the diffracting planes changes as the detector moves through 2θ. Because only planes with the correct orientation diffract X rays, this method is most useful for polycrystalline films having random or nearly random crystallite orientations.

A Double-Crystal Diffractometer (DCD) is useful for characterizing nearly perfect, epitaxial thin films.[4–6] This geometry is similar to the Bragg-Brentano case, but the incident beam is first diffracted from a perfect single crystal (placed near F in Figure 3a). It is thus monochromatic and well collimated. This insures that the measured diffraction peak width of the specimen is narrow, thereby permitting high-resolution measurements. Typically, the detector is fixed near $2\theta_0$, the diffraction angle for the (hkl) planes of interest, and the receiving slits are open to accept a large range in 2θ. The intensity is recorded in a "rocking curve," where the specimen rotates about θ_0. Asymmetric reflections, where the (hkl) planes are not parallel to the substrate can also be measured. Since the diffraction peak widths in DCD measurements are narrow, this method enables accurate determination of very small deviations in d-spacings due to strain.

For ultrathin epitaxial films (less than ~100 Å), GrazingIncidence X-ray Diffraction (GIXD) is the preferred method[6] and has been used to characterize monolayer films. Here the incidence angle is small (~0.5°) and the X rays penetrate only ~100–200 Å into the specimen (see below). The exit angle of the diffracted X rays is also small and structural information is obtained about (hkl) planes perpendicular to the specimen surface. Thus, GIXD complements those methods where structural information is obtained about planes parallel to the surface (e.g., Bragg-Brentano and DCD).

Photographic Methods

Photographic methods[2–4] of characterizing polycrystalline thin films are used to acquire preliminary data and to determine orientational relationships. Guinier and Read cameras are common, although other methods are also used. In a Guinier camera the geometry is the same as for a Seemann-Bohlin diffractometer with a focusing monochromator, except that the "detector" is now a cylinder of film. The geometry of a Read camera is similar to the Bragg-Brentano diffractometer, but the incidence angle is fixed (~5–10°) and the cylindrical film spans a wide range in 2θ.

X-ray topography is a photographic method used to image defects in nearly perfect single crystals.[3, 7] The topograph is a map of the diffracted intensity across the specimen. There are several topographic techniques useful for thin films; [3, 7] we only note a few of their capabilities here. The Berg-Barrett and section methods are simple and give good surface sensitivity. The Lang method (scanning reflection) is more complicated, but large areas can be imaged with good surface sensitivity and spatial resolution. These methods all use a single perfect crystal—the specimen. In the double-crystal method, a reference crystal is used also to produce a monochromatic, collimated incident beam. Although more complicated, this method pro-

vides maximum sensitivity to defects and can provide good surface sensitivity and spatial resolution.

Examples of XRD Characterization of Thin Films

Phase Identification

One of the most important uses of thin-film XRD is phase identification. Although other techniques (e.g., RBS, XPS, and XRF) yield film stoichiometries, XRD provides positive phase identification. This identification is done by comparing the measured d-spacings in the diffraction pattern and, to a lesser extent, their integrated intensities with known standards in the JCPDS Powder Diffraction File (Joint Committee on Powder Diffraction Standards, Swathmore, Pennsylvania, 1986). However, thin films often have a preferred orientation, and this can cause the measured intensities to disagree with the JCPDS file, which are for random orientations. For films containing several phases, the proportion of each phase can be determined from the integrated intensities in the diffraction pattern. If the phases in the film have random orientation or almost complete fiber texture, this determination is simple.[2–4] However, if there is some preferred orientation (incomplete fiber texture), the determination of phase proportions may require integrated intensities at many specimen orientations, which is time consuming. Furthermore, for multiphase specimens, preferred orientation can make positive phase identification difficult, since the integrated intensities may not be useful for phase identification. (For example, peaks that are strong in powder patterns may be weak or completely absent in a specimen with preferred orientation). This difficulty can be particularly acute if data are available only for one specimen orientation (i.e., the Bragg-Brentano geometry) or if the phases produce many diffraction peaks.

Other excellent methods of phase identification include TEM and electron diffraction. These may be more useful for low-Z materials, ultrathin films, and for characterizing small areas, including individual grains. For multiphase films with incomplete texture, these methods and XRD are complementary, since in commonly used geometries, they probe atomic planes perpendicular and parallel to the thin film surface, respectively.

Figure 4 shows an example where XRD is used to unambiguously identify the phases in three high-T_C superconducting thin films.[8] Since the films have nearly complete fiber texture (see below), the identification was simple and was done by comparison to the diffraction patterns from bulk materials. Furthermore, from comparison to standards, the presence of a small amount of CuO is apparent in one film (Figure 4a). We also conclude that the film in Figure 4b consists of approximately equal mixtures of $Tl_2CaBa_2Cu_2O_x$ and $Tl_2Ca_2Ba_2Cu_3O_y$, since it can be reproduced by an approximately equal combination of the patterns in Figures 4a and 4c. Again, because of the strong fiber texture, this determination is straightfor-

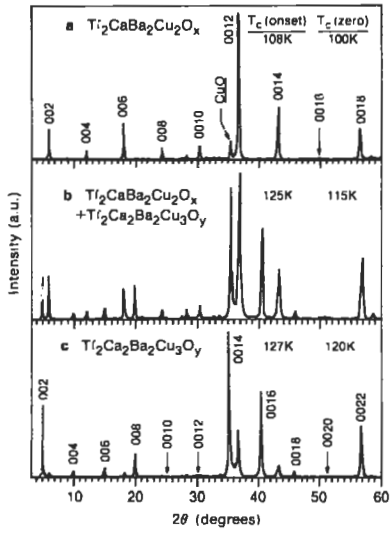

Figure 4 **Diffraction patterns (Bragg-Brentano geometry) of three superconducting thin films (~2-μm thick) annealed for different times.[8] The temperatures for 0 resistance and for the onset of superconductivity are noted.**

ward. Figure 5 shows the XRD pattern from a bilayer film of $Co_{70}Pt_{12}Cr_{18}$/Cr used for magnetic recording.[9] Here the phase of the CoPtCr magnetic media was shown to be hexagonal close packed (hcp) by comparing the measured peaks (including some not shown) with those expected for an hcp solid solution $Co_{70}Pt_{12}Cr_{18}$.

Determination of Strain and Crystallite Size

Diffraction peak positions, and therefore, atomic spacings are accurately measured with XRD, which makes it the best method for characterizing homogeneous and inhomogeneous strains.[2–4, 6, 10] Homogeneous or uniform elastic strain shifts the diffraction peak positions, and if $d_{0,\,hkl}$ is the unstrained d-spacing, $(d_{hkl}-d_{0,\,hk})$ / $d_{0,\,hkl}$ is the component of elastic strain in the (hkl) direction. Figure 6 shows[5] a rocking curve of 2500-Å $Al_{0.88}Ga_{0.12}As$ film on GaAs and illustrates the superb resolution possible with XRD. From the shift in peak positions, one can calculate the difference in d-spacings between the thin film and substrate (in the (100) direction). Although this is only 0.231%, the diffraction peaks from the film and substrate are easily distinguished. Furthermore, the variation in the d-spacing of the film near the film–substrate interface is determined from modeling the data.[5]

Inhomogeneous strains vary from crystallite to crystallite or within a single crystallite and this causes a broadening of the diffraction peaks that increases with $\sin\theta$. Peak broadening is also caused by the finite size of crystallites, but here the broad-

ening is independent of $\sin\theta$. When both crystallite size and inhomogeneous strain contribute to the peak width, these can be separately determined by careful analysis of peak shapes for several diffraction orders (e.g., (111), and (222)).[1–4] Furthermore, the diffraction peak shape can provide information on other types of imperfections (i.e., the presence, extent, and type of stacking faults).[1, 3] If there is no inhomogeneous strain, the crystallite size L is estimated from the peak width $\Delta 2\theta$ with the Scherrer formula:

$$L \sim \frac{\lambda}{(\Delta 2\theta)\cos\theta} \tag{4}$$

Using this and the data in Figure 5, one estimates L ~180 Å for the CoPtCr film.[9] Grain or crystallite size are also determined with TEM through direct imaging. Since this method is a local probe, it can provide more detailed information on imperfections than XRD. Although strain gauges can measure homogeneous strain, there is no good alternative to XRD for strain measurements.

Determination of Preferred Orientation

For polycrystalline films, the amount of preferred orientation can be estimated by comparing the integrated intensities (after correction for geometric factors) to the JCPDS file or the expression for integrated intensity (Equation (3)). If the film has (hkl) fiber texture, then in the Bragg-Brentano geometry, the (hkl) diffraction peak will have a larger relative intensity than expected. Figure 4 shows an example of nearly complete (001) fiber texture in high-T_C thin films, since only the (00l) peaks are observed.[8] For the CoPtCr media (Figure 5), the (002) peak is observed but is weak compared to the (100) and (101) peaks. Thus, the preferred orientation for the (001) axis is to lie in the plane.[9] Although this film possess incomplete fiber texture, phase identification is straightforward, since the reasonable phase possibilities (hcp, fcc, and bcc) are easily distinguished. To obtain a more quantitative determination of preferred orientation, the intensity of an (hkl) peak is measured at different specimen orientations, for example with a pole-figure goniometer.[2] Photographic methods are particularly useful for this, since they provide two-dimensional information, but are less quantitative. For epitaxial films, GIXD and DCD are used to determine thin film orientation. Preferred orientation is also measured with TEM, although less quantitatively.

Film Thickness Determination

The film thickness of epitaxial and highly textured thin films can be measured with XRD.[4, 5] Close to the usual or primary diffraction peaks there are secondary or subsidiary maxima in the diffracted intensity (see Figure 6), which are due to the finite film thickness.[1, 3] The film thickness is inversely proportional to the spacing between these maxima and is easily calculated. X-ray reflectivity is another accurate method for measuring a film's thickness.

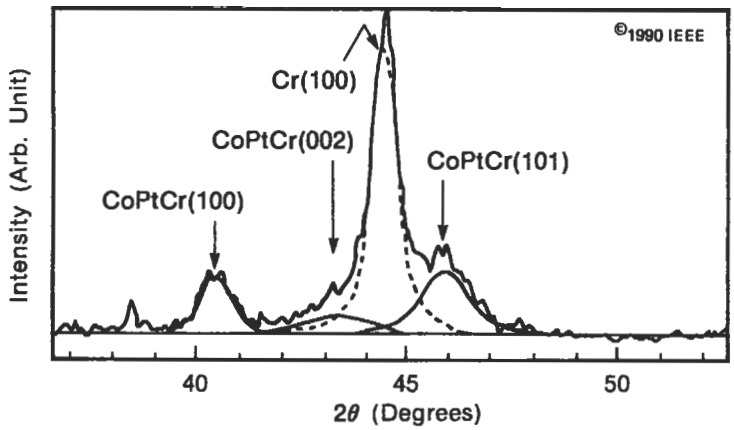

Figure 5 **Bragg-Brentano diffraction pattern for magnetic media used in a demonstration of 1-Gb/in^2 magnetic recording.[9] The lines show a deconvolution of the data into individual diffraction peaks, which are identified.**

Depth-Dependent Information

In most thin-film XRD analyses, depth-dependent structural information is not obtained, but recently such measurements have been performed using a grazing incidence geometry.[11] Since the refractive index for X rays[1, 3] is less than 1, X rays experience total external reflection at incidence angles less than the critical angle for total reflection (α_C). By varying the incidence angle near α_C, the penetration depth of the incident X rays is varied from ~50 Å up to several μm. Since the diffracted X rays originate from different depths, the depth-dependent structure of the specimen may be obtained from diffraction patterns taken at different incidence angles. Depth-dependent structure can also be obtained from TEM, although less quantitatively.

Interdiffusion of bilayered thin films also can be measured with XRD.[12, 13] The diffraction pattern initially consists of two peaks from the pure layers and after annealing, the diffracted intensity between these peaks grows because of interdiffusion of the layers. An analysis of this intensity yields the concentration profile, which enables a calculation of diffusion coefficients, and diffusion coefficients $\sim 10^{-12}$–10^{-15} cm^2/s are readily measured.[12] With the use of multilayered specimens, extremely small diffusion coefficients ($\sim 10^{-23}$ cm^2/s) can be measured with XRD.[12, 13] Alternative methods of measuring concentration profiles and diffusion coefficients include depth profiling (which suffers from artifacts), RBS (which can not resolve adjacent elements in the periodic table), and radiotracer methods (which are difficult). For XRD (except for multilayered specimens), there must be a unique relationship between composition and the d-spacings in the initial films and any solid solutions or compounds that form; this permits calculation of the compo-

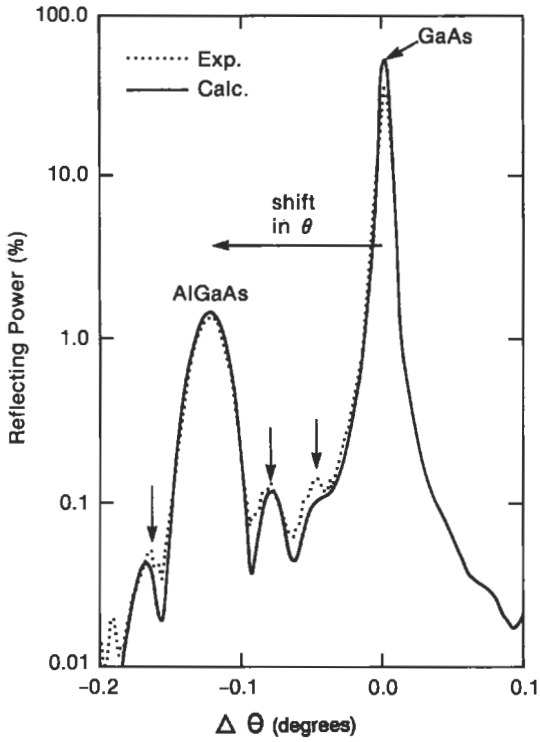

Figure 6 **DCD rocking curves—measured (dashed) and calculated (solid)—of the (400) diffraction peak from $Al_{0.88}Ga_{0.12}As$ on GaAs(100).[5] The arrows mark the subsidiary maxima.**

sition from the diffraction peak positions. On the other hand, the nondestructive nature of XRD makes it a very powerful technique for the measurement of concentration profiles.

X-Ray Topography

X-ray topography[3,7] is used to image defects in nearly perfect epitaxial films and the surface layers of substrates. Typical defects include dislocations, precipitates, fault planes, and local blisters and cracks, and these may be present in the thin film or substrate, or may have been induced into the substrate by the presence of the film. An X-ray topograph is a image of the diffracted intensity across the specimen. Contrast is produced by local variation in the intensity because of changes in the diffraction conditions and is most often due to the strain fields associated with defects. A topograph must be interpreted with the dynamical theory. Although the lateral resolution of X-ray topography (~1 μm) is about 1000 times poorer than TEM, much

smaller strains ($\sim 10^{-6}$) and larger areas (~1–10 cm) can be imaged. Using conventional methods, layers as thin as 1 μm are imaged, but by using grazing incidence angles, the minimum thickness that can be imaged is about 0.1 μm. If the diffraction peaks from a thin film and substrate occur at sufficiently different 2θ, an image of the peak from the thin-film maps only the defects in the film.

Characterization of Multilayered Films

Recently, there has been remarkable progress in the controlled synthesis of multilayered materials,[6, 13] which have a repeating modulation in chemical composition. The atomic structure of multilayers, which influences their properties, is readily studied with XRD. Most XRD investigations have concentrated on structure along the growth direction and this involves measuring atomic planes parallel to the surface, often with Bragg-Brentano or DCD geometries. The wavelength of the modulation in composition (modulation wavelength) and the average strain are determined from the diffraction peak positions; phase identification and measurements of the crystallite size and the preferred orientation are performed as described earlier. A full characterization and understanding of these materials requires accurate knowledge of the interfacial roughness and the composition and position of the atomic planes in a modulation wavelength. This is difficult, since it requires careful analysis of the peak shapes and a complete set of integrated intensities. A determination of the structure in the surface plane can also be important and is performed with GIXD; however, this often is not done. Alternative characterization techniques include neutron diffraction and reflectivity, TEM, EXAFS, LEED, and RHEED, although none of these provide the quantitative detail available with XRD. RHEED, however, is used to monitor multilayer growth in situ.

Characterization of Amorphous Materials

The diffraction pattern from amorphous materials (including many polymers) is devoid of the sharp peaks characteristic of crystals and consists of broad features or halos.[1, 3] Quantitative analysis of XRD data from amorphous materials is complicated but provides important information on the local atomic structure (short-range order), including the bond lengths, the number of neighbors, and the extent of atomic correlations. Since the diffraction from amorphous materials is weak, thick specimens or synchrotron radiation is necessary, particularly for low-Z materials. Many polymers are amorphous or semicrystalline, and for polymeric materials, XRD is used to probe the structure, morphology, and degree of crystallinity.[14] TEM is a widely used alternative for amorphous materials, but is less quantitative and can damage polymers. EXAFS is also widely used and complements XRD but cannot be used for materials composed of only low-Z elements.

Conclusions

XRD is an excellent, nondestructive method for identifying phases and characterizing the structural properties of thin films and multilayers. It is inexpensive and easy to implement. The future will see more use of GIXD and depth dependent measurements, since these provide important information and can be carried out on lab-based equipment (rather than requiring synchrotron radiation). Position sensitive detectors will continue to replace counters and photographic film.

Multilayered materials will become more important in the future, and therefore, their structural characterization using XRD will grow in importance. The use of synchrotron radiation as an analytical tool for thin film characterization will also increase. The unique characteristics of this radiation enable formerly difficult lab-based experiments to be done simply (e.g., GIXD and depth-dependent structural measurements) and permit experiments that are otherwise impossible. These include thin-film energy dispersive XRD, where the incident beam is polychromatic and the diffraction from many atomic planes is obtained simultaneously, and anomalous diffraction, where the abrupt change in the diffracting strength of an element near a particular X-ray energy (an absorption edge) is used to differentiate elements.[2, 3]

Related Articles in the Encyclopedia

TEM, EXAFS, RHEED, LEED, Neutron Diffraction

References

1 B. E. Warren. X-Ray Diffraction. Addison-Wesley, Reading, 1969. A classic text that is complete and thorough, although somewhat dated.

2 B. D. Cullity. Elements of X-Ray Diffraction. Addison-Wesley, Reading, 1978. Another classic text, which is simpler than Warren and emphasizes metallurgy and materials science. A good introduction.

3 L. H. Schwartz and J. B. Cohen. Diffraction from Materials. Springer-Verlag, Berlin, 1987. A recent text that includes X-ray, neutron, and electron diffraction, but emphasizes XRD in materials science. A good introduction and highly recommended.

4 A. Segmuller and M. Murakami. Characterization of Thin Films by X-Ray Diffraction. In: Thin Films from Free Atoms and Particles. (K.J. Klabunde, ed.) Academic Press, Orlando, 1985, p.325 A recent brief review article with many references.

5 V. S. Speriosu, M. A. Nicolet, J. L. Tandon, and Y. C. M. Yeh. Interfacial Strain in AlGaAs Layers on GaAs. J. Appl. Phys. 57, 1377, 1985.

6 A. Segmuller, I. C. Noyan, V. S. Speriosu. X-Ray Diffraction Studies of Thin Films and Multilayer Structures. Prog. Cryst. Growth and Charact. 18, 21, 1989.

7 D. K. Bowen. X-Ray Topography of Surface Layers and Thin Films. In: Advances in X-ray Analysis. (C.S. Barrett, J. V. Gilfrich, R. Jenkins, and P. K. Predecki, eds.) Plenum, New York, 1990, vol. 33, p.13.

8 W. Y. Lee, V. Y. Lee, J. Salem, T. C. Huang, R. Savoy, D. C. Bullock and S. S. P. Parkin. Superconducting TlCaBaCuO Thin Films with Zero Resistance at Temperatures of up to 120K. Appl. Phys. Lett. 53, 329, 1988.

9 T. Y. Yogi, C. Tsang, T. A. Nguyen, K. Ju, G. L. Gorman, and G. Castillo. Longitudinal Magnetic Media for 1Gb / Sq. In. Areal Density. IEEE Trans. Magn. MAG-26, 2271, 1990.

10 A. Segmuller and M. Murakami. X-Ray Diffraction Analysis of Strains and Stresses in Thin Films. In: Analytical Techniques for Thin Films. (K.N. Tu and R. Rosenberg, eds.) Academic, San Diego, 1988, p.143.

11 M. F. Toney and S. Brennan. Structural Depth Profiling of Iron Oxide Thin Films using Grazing Incidence Asymmetric Bragg X-ray Diffraction. J. Appl. Phys. 65, 4763, 1989.

12 M. Murakami, A. Segmuller, K. N. Tu. X-Ray Diffraction Analysis of Diffusion in Thin Films. In: Analytical Techniques for Thin Films. (K. N. Tu and R. Rosenberg, eds.) Academic Press, San Diego, 1988, p.201.

13 P. Dhez and C. Weisbuch. Physics, Fabrication, and Applications of Multilayered Structures. Plenum, New York, 1988.

14 M. Kakudo and N. Kasai. X-ray Diffraction by Polymers. Elsevier, Tokyo, 1972.

4.2 EXAFS

Extended X-Ray Absorption Fine Structure

MARK R. ANTONIO

Contents

Introduction

The discovery of the phenomenon that is now known as extended X-ray absorption fine structure (EXAFS) was made in the 1920s, however, it wasn't until the 1970s that two developments set the foundation for the theory and practice of EXAFS measurements.[1] The first was the demonstration of mathematical algorithms for the analysis of EXAFS data. The second was the advent of intense synchrotron radiation of X-ray wavelengths that immensely facilitated the acquisition of these data. During the past two decades, the use of EXAFS has become firmly established as a practical and powerful analytical capability for structure determination.[2–8]

EXAFS is a nondestructive, element-specific spectroscopic technique with application to all elements from lithium to uranium. It is employed as a direct probe of the atomic environment of an X-ray absorbing element and provides chemical bonding information. Although EXAFS is primarily used to determine the local structure of bulk solids (e.g., crystalline and amorphous materials), solid surfaces, and interfaces, its use is not limited to the solid state. As a structural tool, EXAFS complements the familiar X-ray diffraction technique, which is applicable only to crystalline solids. EXAFS provides an atomic-scale perspective about the X-ray absorbing element in terms of the numbers, types, and interatomic distances of neighboring atoms.

EXAFS is part of the field of X-ray absorption spectroscopy (XAS), in which a number of acronyms abound. An X-ray absorption spectrum contains EXAFS data as well as the X-ray absorption near-edge structure, XANES (alternatively called the near-edge X-ray absorption fine structure, NEXAFS). The combination of XANES (NEXAFS) and EXAFS is commonly referred to as X-ray absorption fine structure, or XAFS. In applications of EXAFS to surface science, the acronym SEXAFS, for surface-EXAFS, is used. The principles and analysis of EXAFS and SEXAFS are the same. See the article following this one for a discussion of SEXAFS and NEXAFS.

Experimental Aspects

An EXAFS experiment involves the measurement of the X-ray photoabsorption of a selected element as a function of energy above its core-shell electron binding energy. The most direct measurement of EXAFS is the transmission method, wherein the sample is placed in the X-ray beam and the incident and transmitted X-ray intensities, I_0 and I_t, respectively, are recorded (see Figure 1). The measurement of I_0 and I_t is accomplished with two ion chamber proportional counters that are gas filled (typically with nitrogen and argon) to provide about 10–20% absorption of I_0 and 80–90% absorption of I_t. As shown in Figure 1, it is useful to have a third ion chamber for simultaneous measurements of a reference material (e.g., a thin metal foil) to maintain accurate energy calibration throughout the course of experiment. For successful transmission measurements, the ideal sample thickness x is one absorption length, i.e., $x = 1/[(\mu/\rho)\rho]$; here μ/ρ is the total mass absorption coefficient and ρ is the density. Transmission EXAFS data for samples with larger absorption lengths can be seriously distorted and are not suitable for analysis.[9] Transmission EXAFS data are displayed in the form $\ln(I_0/I_t)$ versus incident X-ray energy, as shown in Figure 2.

A wide selection of metal reference foils and powder films of ideal thickness for tranmission EXAFS is available from The EXAFS Materials Company, Danville, CA, USA. The transmission method is well-suited for *in situ* measurements of materials under industrially relevant conditions of extreme temperature and controlled atmosphere. Specially designed reactors for catalysis experiments and easy-

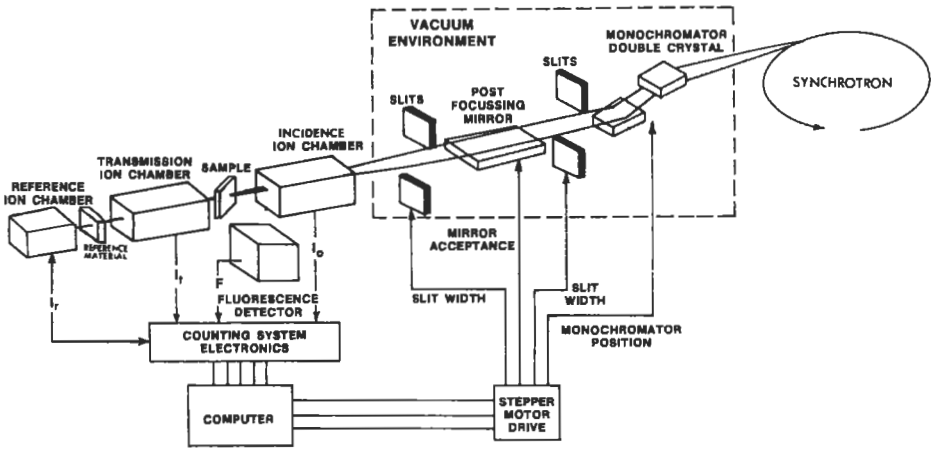

Figure 1 **Schematic view of a typical EXAFS experiment at a synchrotron radiation facility. Note that it is possible to record transmission and fluorescence EXAFS simultaneously with reference EXAFS.**

to-use detectors are commercially available from The EXAFS Company, Seattle, WA, USA.

In addition to transmission, EXAFS data can be recorded through the detection of

1 X-ray fluorescence
2 Electron yield
3 Ion yield
4 Optical luminescence
5 Photoconductivity
6 Photoacoustic signals.

The last three detection schemes apply only under very special circumstances.[3–6] Transmission EXAFS is strictly a probe of bulk structure, i.e., more than about a thousand monolayers. The electron- and ion-yield detection methods, which are used in reflection rather than transmission schemes, provide surface sensitivity, ~1–1,000 Å, and are inherently insensitive to bulk structure. X-ray fluorescence EXAFS has the widest range of sensitivity—from monolayer to bulk levels. The combination of electron or ion yield and transmission EXAFS measurements can provide structural information about the X-ray absorbing element at the surface and in the bulk, respectively, of a sample.

Without exception, the highest quality EXAFS data are acquired at synchrotron radiation facilities. There are 20 operational facilities throughout the world.[10] Each has unique instrumentation: The interested user is encouraged to contact the facil-

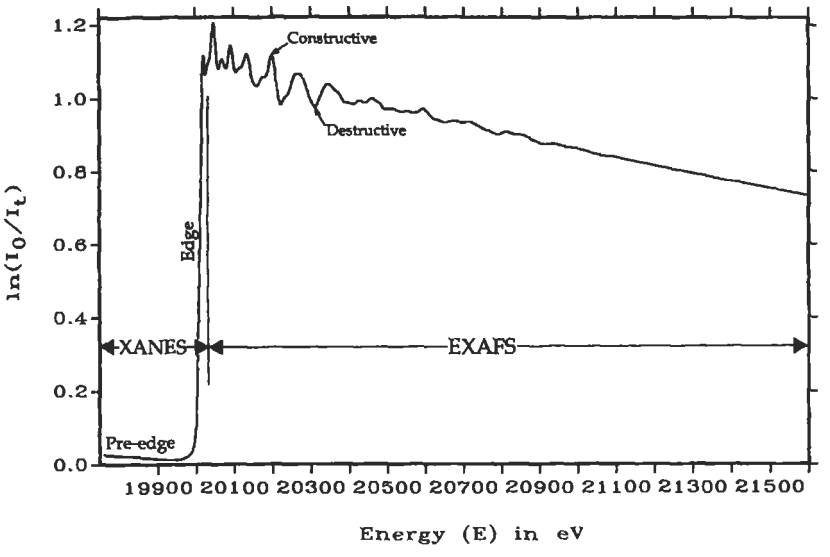

Figure 2 **Molybdenum K-edge X-ray absorption spectrum, $\ln(I_0/I_t)$ versus X-ray energy (eV), for molybdenum metal foil (25-μm thick), obtained by transmission at 77 K with synchrotron radiation. The energy-dependent constructive and destructive interference of outgoing and backscattered photoelectrons at molybdenum produces the EXAFS peaks and valleys, respectively. The pre-edge and edge structures marked here are known together as X-ray absorption near edge structure, XANES and EXAFS are provided in a new compilation of literature entitled *X-ray Absorption Fine Structure* (S.S. Hasain, ed.) Ellis Horwood, New York, 1991.**

ity for detailed information, such as is available in Gmur.[11] In general, "hard" X-ray beam lines (approximately ≥ 2,000 eV) employ flat-crystal monochromators to scan the X-ray energy over the region of interest, whereas "soft" X-ray beam lines (approximately ≤ 1,000 eV) employ grating-type monochromators for the same purpose. The monochromatization of X rays with energies between approximately 1,000 and 2,000 eV is a difficult problem—neither crystal nor grating monochromators work particularly well.

Basic Principles

Both inner-shell (K and L) and outer-shell (M, N, etc.) electrons can be excited by the absorption of X rays and by the inelastic scattering of electrons. In either instance, at an electron binding energy characteristic of an element in a sample,

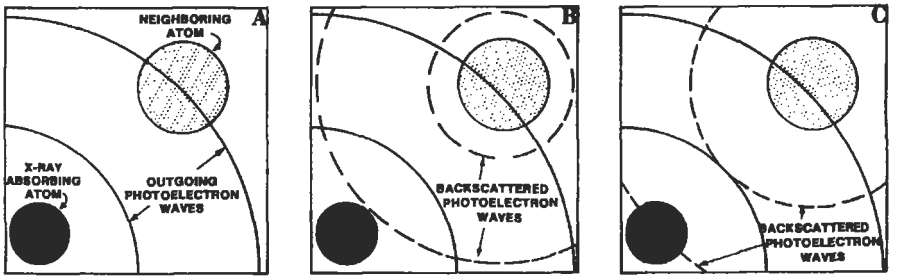

Figure 3 **Schematic illustration of the EXAFS phenomenon: (A) outgoing photoelectron (solid curve) from X-ray absorbing atom; (B) destructive interference at the absorbing atom between outgoing (solid curve) and backscattered (dashed curve) photoelectron from neighboring atom; (C) constructive interference at the absorbing atom between outgoing (solid curve) and backscattered (dashed curve) photoelectron from neighboring atom. Adapted from T. M. Hayes and J. B. Boyce. *Solid State Phys.* 37, 173, 1982.**

absorption occurs and a steeply rising absorption edge is observed. For example, molybdenum exhibits an X-ray absorption edge at 20,000 eV, which is the 1s electron binding energy (K edge) , see Figure 2. The pre-edge and edge features are collectively referred to as XANES or NEXAFS, depending upon the application. These data are valuable for probing the site symmetry and valence of the X-ray absorbing element, but will not be discussed further here.

For X-ray energies greater than the binding energy, the absorption process leads to the excitation of the core electron to the ionization continuum. The resulting photoelectron wave propagates from the X-ray absorbing atom and is scattered by the neighboring atoms, as illustrated in Figure 3. The EXAFS spectrum results from the constructive and destructive interference between the outgoing and incoming photoelectron waves at the absorbing atom. The interference gives rise to the modulatory structure (i.e., peaks and valleys) of the X-ray absorption versus incident X-ray energy, as in Figure 2. This process also makes EXAFS unique—the absorbing atom acts as both the source and detector of the interference that is the EXAFS phenomenon.

EXAFS is a probe of the structural distribution, e.g., interatomic distances, numbers of neighboring atoms (the so-called coordination number), and degree of disorder—and identity of atoms in the immediate vicinity (~5 Å) of the X-ray absorbing atom. A simplified schematic representation of several descriptive features of EXAFS is presented in Figure 4. The frequency of EXAFS oscillations is related to the distance between the X-ray absorbing atom (filled circles) and the backscattering atoms (open circles). For large interatomic distances ($R_1 > R_2$), the EXAFS has shorter periods (higher frequencies) than for small distances; see curves

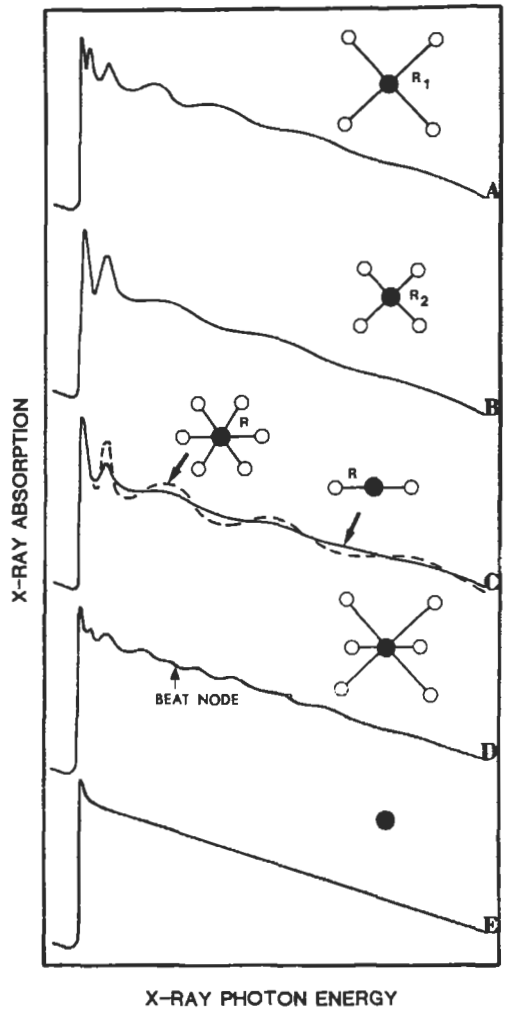

Figure 4 **Descriptive aspects of EXAFS: Curves A–E are discussed in the text. Adapted from J. Stohr. In: *Emission and Scattering Techniques: Studies of Inorganic Molecules, Solids, and Surfaces.* (P. Day, ed.) Kluwer, Norwell, MA, 1981.**

A and B, respectively, in Figure 4. The periodicity is also related to the identity of the absorbing and backscattering elements. Each has unique phase shifts.[12]

EXAFS has an energy-dependent amplitude that is just a few % of the total X-ray absorption. This amplitude is related to the number, type, and arrangement of backscattering atoms around the absorbing atom. As illustrated in Figure 4 (curve C), the EXAFS amplitude for backscattering by six neighboring atoms at a distance R is greater than that for backscattering by two of the same atoms at the same distance. The amplitude also provides information about the identity of the

backscattering element—each has a unique scattering function[12]—and the number of different atomic spheres about the X-ray absorbing element. As shown in Figure 4, the EXAFS for an atom with one sphere of neighbors at a single distance exhibits a smooth sinusoidal decay (see curves A–C), whereas that for an atom with two (or more) spheres of neighbors at different distances exhibits beat nodes due to superposed EXAFS signals of different frequencies (curve D).

The EXAFS amplitude is also related to the Debye-Waller factor, which is a measure of the degree of disorder of the backscattering atoms caused by dynamic (i.e., thermal–vibrational properties) and static (i.e., inequivalence of bond lengths) effects. Separation of these two effects from the total Debye-Waller factor requires temperature-dependent EXAFS measurements. In practice, EXAFS amplitudes are larger at low temperatures than at high ones due to the reduction of atomic motion with decreasing temperature. Furthermore, the amplitude for six backscattering atoms arranged symmetrically about an absorber at some average distance is larger than that for the same number of backscattering atoms arranged randomly about an absorber at the same average distance. Static disorder about the absorbing atom causes amplitude reduction. Finally, as illustrated in Figure 4 (curve E), there is no EXAFS for an absorbing element with no near neighbors, such as for a noble gas.

Data Analysis

Because EXAFS is superposed on a smooth background absorption μ_0 it is necessary to extract the modulatory structure μ from the background, which is approximated through least-squares curve fitting of the primary experimental data with polynomial functions (i.e., $\ln(I_0/I_t)$ versus E in Figure 2).[7, 12] The EXAFS spectrum χ is obtained as $\chi = [\mu-\mu_0]/\mu_0$. Here χ, μ, and μ_0 are functions of the photoelectron wave vector $\mathbf{k}$ (Å^{-1}), where $k = [0.263\ (E-E_0)]^{1/2}$; E_0 is the experimental energy threshold chosen to define the energy origin of the EXAFS spectrum in k-space. That is, $k = 0$ when the incident X-ray energy E equals E_0, and the photoelectron has no kinetic energy.

EXAFS data are multiplied by k^n (n = 1, 2, or 3) to compensate for amplitude attenuation as a function of k, and are normalized to the magnitude of the edge jump. Normalized, background-subtracted EXAFS data, $k^n\chi(k)$ versus k (such as illustrated in Figure 5), are typically Fourier transformed without phase shift correction. Fourier transforms are an important aspect of data analysis because they relate the EXAFS function $k^n\chi(k)$ of the photoelectron wavevector $\mathbf{k}$ (Å^{-1}) to its complementary function $\Phi_n(r')$ of distance r'(Å). Hence, the Fourier transform provides a simple physical picture, a pseudoradial distribution function, of the environment about the X-ray absorbing element. The contributions of different coordination spheres of neighbors around the absorber appear as peaks in the Fourier transform. The Fourier transform peaks are always shifted from the true distances r to shorter ones r' due to the effect of a phase shift, which amounts to ~0.2–0.5 Å, depending upon the absorbing and backscattering atom phase functions.

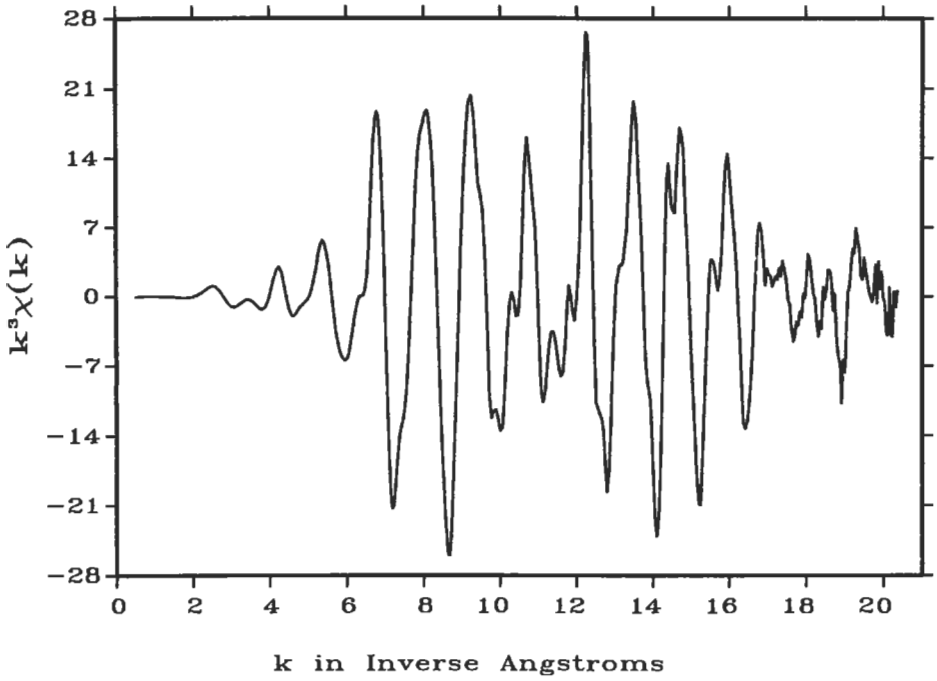

Figure 5 **Background-subtracted, normalized, and k^3-weighted Mo K-edge EXAFS, $k^3\chi(k)$ versus k (Å^{-1}), for molybdenum metal foil obtained from the primary experimental data of Figure 2 with E_0 = 20,025 eV.**

The Fourier transform of the EXAFS of Figure 5 is shown in Figure 6 as the solid curve: It has two large peaks at 2.38 and 2.78 Å as well as two small ones at 4.04 and 4.77 Å. In this example, each peak is due to Mo–Mo backscattering. The peak positions are in excellent correspondence with the crystallographically determined radial distribution for molybdenum metal foil (bcc)—with Mo–Mo interatomic distances of 2.725, 3.147, 4.450, and 5.218 Å, respectively. The Fourier transform peaks are phase shifted by ~0.39 Å from the true distances.

To extract structural parameters (e.g. interatomic distances, Debye-Waller factors, and the number of neighboring atoms) with greater accuracy than is possible from the Fourier transform data alone, nonlinear least-squares minimization techniques are applied to fit the EXAFS or Fourier transform data with a semiempirical, phenomenological model of short-range, single scattering.[7, 12] Fourier-filtered EXAFS data are well suited for the iterative refinement procedure. High-frequency noise and residual background apparent in the experimental data are effectively removed by Fourier filtering methods. These involve the isolation of the peaks of interest from the total Fourier transform with a filter function, as illustrated by the dashed curve in Figure 6. The product of the smooth filter with the real and imagi-

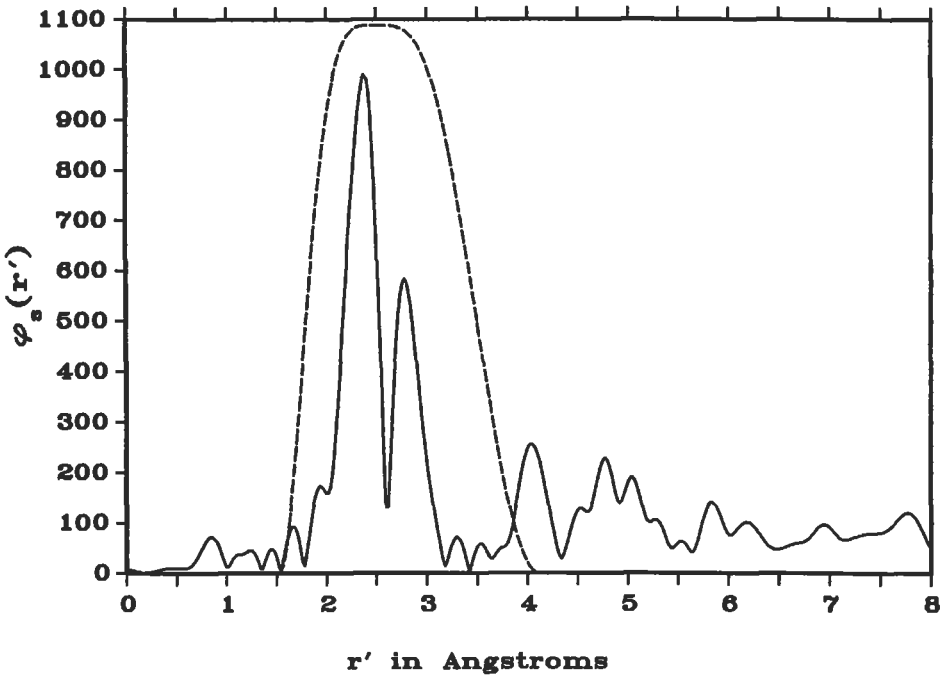

Figure 6 **Fourier transform (solid curve), $\Phi_3(r')$ versus r' (Å, without phase-shift correction), of the Mo K-edge EXAFS of Figure 5 for molybdenum metal foil. The Fourier filtering window (dashed curve) is applied over the region ~1.5–4.0 Å to isolate the two nearest Mo–Mo peaks.**

nary parts of the Fourier transform on the selected distance range is then Fourier inverse-transformed back to wavevector space to provide Fourier-filtered EXAFS, as illustrated by the solid curve of Figure 7. For curve fitting, phase shifts and back-scattering amplitudes are fixed during the least-squares cycles. These can be obtained readily from theoretical or, alternatively, empirical tabulations.[12] The best fit (dashed curve) to the Fourier-filtered EXAFS data (solid curve) of the first two coordination spheres of molybdenum metal is shown in Figure 7.

Capabilities and Limitations

The classical approach for determining the structures of crystalline materials is through diffraction methods, i.e., X-ray, neutron-beam, and electron-beam techniques. Diffraction data can be analyzed to yield the spatial arrangement of all the atoms in the crystal lattice. EXAFS provides a different approach to the analysis of atomic structure, based not on the diffraction of X rays by an array of atoms but rather upon the absorption of X rays by individual atoms in such an array. Herein lie the capabilities and limitations of EXAFS.

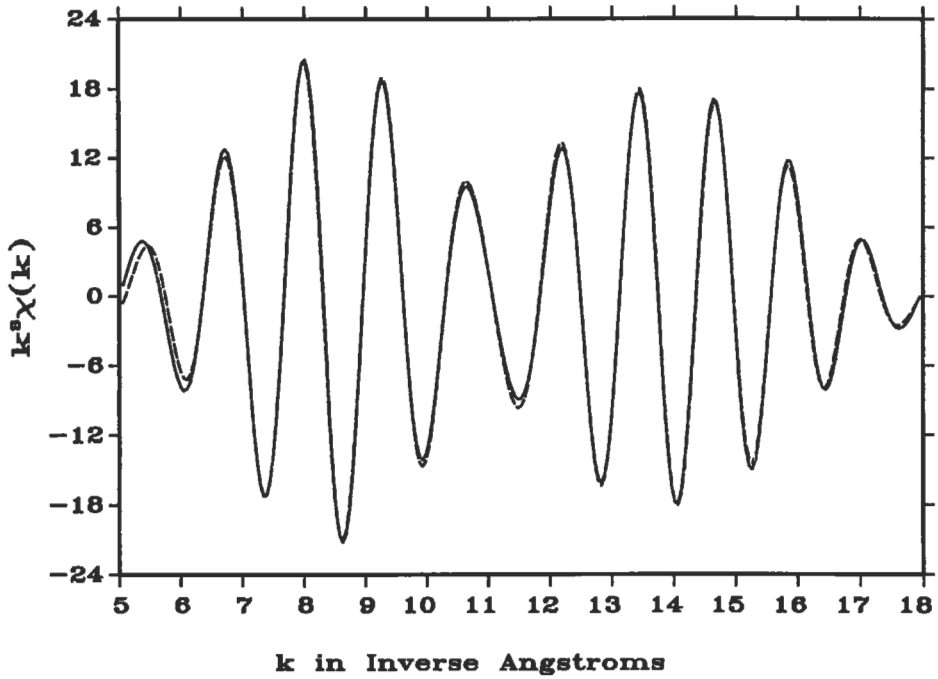

Figure 7 **Fourier-filtered Mo K-edge EXAFS, $k^3\chi(k)$ versus k (Å^{-1}) (solid curve), for molybdenum metal foil obtained from the filtering region of Figure 6. This data is provided for comparison with the primary experimental EXAFS of Figure 5. The two-term Mo–Mo best fit to the filtered data with theoretical EXAFS amplitude and phase functions is shown as the dashed curve.**

Because diffraction methods lack the element specificity of EXAFS and because EXAFS lacks the power of molecular-crystal structure solution of diffraction, these two techniques provide complementary information. On the one hand, diffraction is sensitive to the stereochemical short- and long-range order of atoms in specific sites averaged over the different atoms occupying those sites. On the other hand, EXAFS is sensitive to the radial short-range order of atoms about a specific element averaged over its different sites. Under favorable circumstances, stereochemical details (i.e., bond angles) may be determined from the analysis of EXAFS for both oriented and unoriented samples.[12] Furthermore, EXAFS is applicable to solutions and gases, whereas diffraction is not. One drawback of EXAFS concerns the investigation of samples wherein the absorbing element is in multiple sites or multiple phases. In either case, the results obtained are for an average environment about all of the X-ray absorbing atoms due to the element-specific site averaging of structural information. Although not common, site-selective EXAFS is possible.[3]

Unlike traditional surface science techniques (e.g., XPS, AES, and SIMS), EXAFS experiments do not routinely require ultrahigh vacuum equipment or electron- and ion-beam sources. Ultrahigh vacuum treatments and particle bombardment may alter the properties of the material under investigation. This is particularly important for accurate valence state determinations of transition metal elements that are susceptible to electron- and ion-beam reactions. Nevertheless, it is always more convenient to conduct experiments in one's own laboratory than at a synchrotron radiation facility, which is therefore a significant drawback to the EXAFS technique. These facilities seldom provide timely access to beam lines for experimentation of a proprietary nature, and the logistical problems can be overwhelming.

Although not difficult, the acquisition of EXAFS is subject to many sources of error, including those caused by poorly or improperly prepared specimens, detector nonlinearities, monochromator artifacts, energy calibration changes, inadequate signal-to-noise levels, X-ray beam induced damage, etc.[9] Furthermore, the analysis of EXAFS can be a notoriously subjective process: an accurate structure solution requires the generous use of model compounds with known structures.[7, 12]

Applications

EXAFS has been used to elucidate the structure of adsorbed atoms and small molecules on surfaces; electrode–electrolyte interfaces; electrochemically produced solution species; metals, semiconductors, and insulators; high-temperature superconductors; amorphous materials and liquid systems; catalysts; and metalloenzymes. Aspects of the applications of EXAFS to these (and other) systems are neatly summarized in References 1–9, and will not be repeated here. It is important to emphasize that EXAFS experiments are indispensable for *in situ* studies of materials, particulary catalysts[3–9] and electrochemical systems.[13] Other techniques that have been successfully employed for *in situ* electrochemical studies include ellipsometry, X-ray diffraction, X-ray standing wave detection, Mossbauer-effect spectroscopy, Fourier-transform infrared spectroscopy, UV-visible reflectance spectroscopy, Raman scattering, and radiotracer methods. Although the established electrochemical technique of cyclic voltammetry is a true *in situ* probe, it provides little direct information about atomic structure and chemical bonding. EXAFS spectroelectrochemistry is capable of providing such information.[13] In this regard, thin oxide films produced by passivation and corrosion phenomena have been the focus of numerous EXAFS investigations.

It is known that thin (~20 Å) passive films form on iron, nickel, chromium, and other metals. In aggressive environments, these films provide excellent corrosion protection to the underlying metal. The structure and composition of passive films on iron have been investigated through iron K-edge EXAFS obtained under a variety of conditions,[8, 14] yet there is still some controversy about the exact nature of

passive films on iron. The consensus is that the passive film on iron is a highly disordered form of γ-FeOOH. Unfortunately, the majority of EXAFS studies of passive films have been on chemically passivated metals: Electrochemically passivated metals are of greater technological significance. In addition, the structures of passive films after attack by chloride ions and the resulting corrosion formations have yet to be thoroughly investigated with EXAFS.

Conclusions

Since the early 1970s, the unique properties of synchrotron radiation have been exploited for EXAFS experiments that would be impossible to perform with conventional sources of X-radiation. This is not surprising given that high-energy electron synchrotrons provide 10,000 times more intense continuum X-ray radiation than do X-ray tubes. Synchrotron radiation has other remarkable properties, including a broad spectral range, from the infrared through the visible, vacuum ultraviolet, and deep into the X-ray region; high polarization; natural collimation; pulsed time structure; and a small source size. As such, synchrotron radiation facilities provide the most useful sources of X-radiation available for EXAFS.

The future of EXAFS is closely tied with the operation of existing synchrotron radiation laboratories and with the development of new ones. Several facilities are now under construction throughout the world, including two in the USA (APS, Argonne, IL, and ALS, Berkeley, CA) and one in Europe (ESRF, Grenoble, France). These facilities are wholly optimized to provide the most brilliant X-ray beams possible—10,000 times more brilliant than those available at current facilities! The availability of such intense synchrotron radiation over a wide range of wavelengths will open new vistas in EXAFS and materials characterization. Major advances are anticipated to result from the accessibility to new frontiers in time, energy, and space. The tremendous brilliance will facilitate time-resolved EXAFS of processes and reactions in the microsecond time domain; high-energy resolution measurements throughout the electromagnetic spectrum; and microanalysis of materials in the submicron spatial domain, which is hundreds of times smaller than can be studied today. Finally, the new capabilities will provide unprecedented sensitivity for trace analysis of dopants and impurities.

Related Articles in the Encyclopedia

NEXAFS, EELS, LEED, Neutron Diffraction, AES, and XPS

References

1 *EXAFS Spectroscopy: Techniques and Applications.* (B. K. Teo and D. C. Joy, eds.) Plenum, New York, 1981. Contains historical items and treatments of EXELFS, the electron-scattering counterpart of EXAFS.

2 P. A. Lee, P. H. Citrin, P. Eisenberger, and B. M. Kincaid. Extended X-ray Absorption Fine Structure—Its Strengths and Limitations as a Structural Tool. *Rev. Mod. Phys.* **53,** 769, 1981.

3 *XAFS V, Proceedings of the Fifth International Conference on X-ray Absorption Fine Structure.* (J. M. de Leon, E. A. Stern, D. E. Sayers, Y. Ma, and J. J. Rehr, eds.) North-Holland, Amsterdam, 1989. Also in *Physica B.* **158,** 1989. "Report of the International Workshop on Standards and Criteria in X-ray Absorption Spectroscopy" (pp. 701–722) is essential reading.

4 *EXAFS and Near Edge Structure IV. Proceedings of the International Conference.* (P. Lagarde, D. Raoux, and J. Petiau, eds.) *J. De Physique,* **47**, Colloque C8, Suppl. 12, 1986, Volumes 1 and 2.

5 *EXAFS and Near Edge Structure III. Proceedings of an International Conference.* (K. O. Hodgson, B. Hedman, and J. E. Penner-Hahn, eds.) Springer, Berlin, 1984.

6 *EXAFS and Near Edge Structure. Proceedings of the International Conference.* (A. Bianconi, L. Incoccia, and S. Stipcich, eds.) Springer, Berlin, 1983.

7 *X-Ray Absorption. Principles, Applications, Techniques of EXAFS, SEXAFS and XANES.* (D. C. Koningsberger and R. Prins, eds.) Wiley, New York, 1988.

8 Structure of Surfaces and Interfaces as Studied Using Synchrotron Radiation. *Faraday Discussions Chem. Soc.* 89, 1990. A lively and recent account of studies in EXAFS, NEXAFS, SEXAFS, etc.

9 *Applications of Synchrotron Radiation.* (H. Winick, D. Xian, M. H. Ye, and T. Huang, eds.) Gordon and Breach, New York, 1988, Volume 4. F. W. Lytle provides (pp. 135–223) an excellent tutorial survey of experimental X-ray absorption spectroscopy.

10 H. Winick and G. P. Williams. Overview of Synchrotron Radiation Sources World-wide. *Synchrotron Radiation News.* **4,** 23, 1991.

11 *National Synchrotron Light Source User's Manual: Guide to the VUV and X-Ray Beam Lines.* (N. F. Gmur ed.) BNL informal report no. 45764, 1991.

12 B. K. Teo. *EXAFS: Basic Principles and Data Analysis.* Springer, Berlin, 1986.

13 L. R. Sharpe, W. R. Heineman, and R. C. Elder. EXAFS Spectroelectrochemistry. *Chem. Rev.* **90,** 705, 1990.

14 *Passivity of Metals and Semiconductors.* (M. Froment, ed.) Elsevier, Amsterdam, 1983.

4.3 SEXAFS / NEXAFS

Surface Extended X-Ray Absorption Fine Structure and Near Edge X-Ray Absorption Fine Structure

DAVID NORMAN

Contents

Introduction

SEXAFS is a research technique providing the most precise values obtainable for adsorbate–substrate bond lengths, plus some information on the number of nearest neighbors (coordination numbers). Other methods for determining the quantitative geometric structure of atoms at surfaces, described elsewhere in this volume (e.g., LEED, RHEED, MEIS, and RBS), work only for single-crystal substrates having atoms or molecules adsorbed in a regular pattern with long-range order within the adsorbate plane. SEXAFS does not suffer from these limitations. It is sensitive only to local order, sampling a short range within a few Å around the absorbing atom.

SEXAFS can be measured from adsorbate concentrations as low as ~0.05 monolayers in favorable circumstances, although the detection limits for routine use are several times higher. By using appropriate standards, bond lengths can be determined as precisely as ±0.01 Å in some cases. Systematic errors often make the accu-

racy much poorer than the precision, with more realistic estimates of ±0.03 Å or worse.

NEXAFS has become a powerful technique for probing the structure of molecules on surfaces. Observation of intense resonances near the X-ray absorption edge can indicate the type of bonding. On a flat surface, the way in which the resonances vary with angle of the specimen can be analyzed simply to give the molecular orientation, which is precise to within a few degrees. The energies of resonances allow one to estimate the intramolecular bond length, often to within ±0.05 Å. Useful NEXAFS can be seen for concentrations as low as ~0.01 monolayer in favorable cases.

The techniques can be applied to almost any adsorbate on almost any type of solid sample—metal, semiconductor or insulator. Light adsorbates—say, from C through Al—are more difficult to study than heavier ones because their absorption edges occur at low photon energies that are technically more difficult to produce. The technique samples all absorbing atoms of the same type, and averages over them, so that good structural information is obtained only when the adsorbates uniquely occupy equivalent sites. Thus it is not easy to examine clean surfaces, where the EXAFS signal from surface atoms is overwhelmed by that from the bulk. The best way to study such samples is with X rays incident on the sample at a grazing angle so that they interact only in a region close to the surface: by varying the angle, the probing depth can be changed somewhat. The reviews of SEXAFS and NEXAFS[1–5] should be consulted for more details.

Basic Principles of X-ray Absorption

The physical processes of X-ray absorption are depicted schematically in Figure 1. The energies of discrete core levels are uniquely determined by the atom type (as in XPS or AES), so tuning the photon energy to a particular core level gives an *atom-specific* probe. When the photon energy equals the binding energy of the electron in a core level, a strong increase in absorption is seen, which is known as the absorption edge. The absorbed photon gives its energy to a photoelectron that propagates as a wave. In a molecule or solid, part of this photoelectron wave may be backscattered from neighboring atoms, the backscattered wave interfering constructively or destructively with the outgoing wave. Thus one gets a spectrum of absorption as a function of photon energy that contains wiggles (EXAFS) superimposed on a smooth background. The amplitude of the EXAFS wiggles depends on the number of neighbors, the strength of their scattering and the static and dynamic disorder in their position. The frequency of the EXAFS wiggles depends on the wavevector k of the photoelectrons (related to their kinetic energy) and the distance to neighboring atoms. The frequency is inversely related to the nearest neighbor separation, with a short distance giving widely spaced wiggles and vice versa.

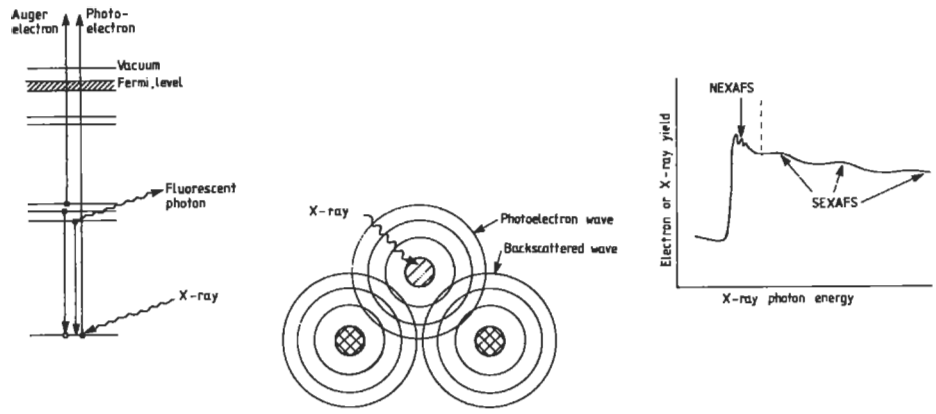

Figure 1 **Basic physical principles of X-ray absorption. As in XPS/ESCA, absorption of a photon leads to emission of a photoelectron. This photoelectron, propagating as a wave, may be scattered from neighboring atoms. The backscattered wave interferes constructively or destructively with the outgoing wave, depending on its wavelength and the distance to neighboring atoms, giving wiggles in the measured absorption spectrum.**

EXAFS can be used to study surfaces or bulk samples. Ways of making the technique surface-sensitive are spelled out below. EXAFS gives a spherical average of information in a shell around an absorbing atom. For an anisotropic sample with a polarized photon beam, one gets a searchlight effect, where neighbors in directions along that of the polarization vector **E** (perpendicular to the direction of the X rays) are selectively picked out. For studies on flat surfaces the angular variation of the EXAFS intensity is one of the best methods of identifying an adsorption site. The form of the backscattering amplitude depends on atomic number, differing between atoms in different rows of the periodic table,[5] and this helps one to determine which atoms in a compound are nearest neighbors.

Phase Shifts

When an electron scatters from an atom, its phase is changed so that the reflected wave is not in phase with the incoming wave. This changes the interference pattern and hence the apparent distance between the two atoms. Knowledge of this phase shift is the key to getting precise bond lengths from SEXAFS. Phase shifts depend mainly on which atoms are involved, not on their detailed chemical environment, and should therefore be transferable from a known system to unknown systems. The phase shifts may be obtained from theoretical calculations, and there are published tabulations, but practically it is desirable to check the phase shifts using

model compounds: the idea is to take a sample of known composition and crystallography, measure its EXAFS spectrum and analyze it to determine a phase shift ϕ. The model compound should ideally contain the same absorber and backscatterer atoms as the unknown, and in the same chemical state. If this is not possible, the next best option is to use a model whose absorber and a backscatterer are neighboring elements in the periodic table to those in the unknown sample, although for highest precision the backscatterer should be the same as in the unknown.

One must be sure of the purity of the model compound. It may have deteriorated (for example, by reaction or water absorption), its surface may not have the same composition as the bulk, or it may not be of the correct crystallographic phase. It is tempting to use single crystals to be sure of the geometric structure, but noncubic crystals give angle-dependent spectra. The crystallography of any compound should be checked with XRD.

Experimental Details

There are several ways to make a SEXAF/NEXAFS measurement surface sensitive.

1. By using dispersed samples, the surface-to-bulk ratio is increased, and standard methods of studying "bulk" samples will work (see the article on EXAFS).
2. By making the X rays incident on the sample at shallow angles (usually a fraction of a degree), they see only the near-surface region, some 20–50 Å deep. The angle of incidence can be varied, allowing crude depth profiling, but the penetration is crucially dependent on the flatness of the reflecting surface, and large homogeneous samples are needed. This is potentially a useful technique for studying buried interfaces, where the signal will come predominantly from the interface if the substrate is more dense than the overlayer. This method has been little tried in the soft X-ray region but should work well, since the critical angle is larger than for hard X rays.
3. Since X-ray absorption is an atom-specific process, any atoms known to be, or deliberately placed, on a solid consisting of different atoms can be studied with high sensitivity.
4. The absorption may be monitored via a secondary decay process that is surface-sensitive, such as the emission of Auger electrons, which have a well-defined energy and a short mean free path.

X-Ray Sources

The only X-ray source with sufficient intensity for surface measurements is synchrotron radiation. Synchrotron radiation is white light, including all wavelengths from the infrared to X rays. A spectroscopy experiment needs a particular wavelength (photon energy) to be selected with a monochromator and scanned through

the spectrum. For EXAFS, a range is needed of at least 300 eV above the absorption edge that does not contain any other edges, such as those from coadsorbates, the substrate, or from higher order light (unwanted X rays from the monochromator with two, three, or more times the desired energy). NEXAFS needs a clear range of perhaps 25–30 eV above the edge. Perusal of a table of energy levels is essential.[6] Photon energies from about 4 keV to 15 keV are easiest to use, where X-ray windows allow sample chambers to be separated from the monochromator. Energies below about 1800 eV are technically the most difficult, requiring ultrahigh vacuum monochromators directly connected to the sample chamber. K edges are easiest to interpret, but $L_{2,3}$ edges can be used: line widths are much broader at L_1 edges, and states such as M_5 may have an absorption edge too wide to be usable for EXAFS.

Detection Methods

The experiment consists of measuring the intensity of photons incident on the sample, and the proportion of them that is absorbed. Most SEXAFS experiments detect the X-ray absorption coefficient indirectly by measuring the fluorescence or Auger emission that follows photon absorption. (See the articles on AES and XRF.) The various electron or photon detection schemes should be tested to see which one gives the best data in each case. Measuring all electrons, the total electron yield (TEY), or those in a selected bandpass, the partial electron yield (PEY), will give higher signals but poorer sensitivity than the Auger electron yield (AEY). Fluorescence yields (FYs) are low for light elements, so their measurement usually gives weak signals, but the background signal is usually low, in which case FY will give high sensitivity. FY is the technique of choice for insulating samples that may charge up and confuse electron detection. FY also allows for experiments in which the sample is in an environment other than the high vacuum needed for electrons. With suitable windows, surface reactions may be followed *in situ*, for instance in a high-pressure chamber or an electrochemical cell, although this type of work is yet in its infancy.

Electron Excitation

The advantages of SEXAFS/NEXAFS can be negated by the inconvenience of having to travel to synchrotron radiation centers to perform the experiments. This has led to attempts to exploit EXAFS-like phenomena in laboratory-based techniques, especially using electron beams. Despite doubts over the theory there appears to be good experimental evidence[7] that electron energy loss fine structure (EELFS) yields structural information in an identical manner to EXAFS. However, few EELFS experiments have been performed, and the technique appears to be more taxing than SEXAFS.

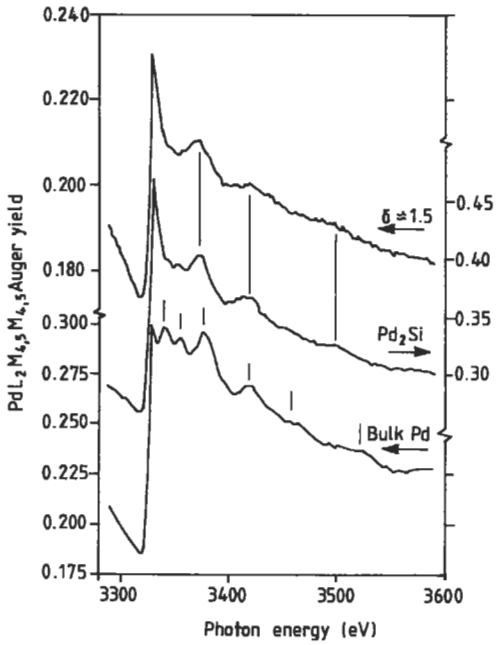

Figure 2 **Surface EXAFS spectra above the Pd L_2-edge for a 1.5 monolayer evaporated film of Pd on Si(111) and for bulk palladium silicide, Pd_2Si and metallic Pd.**

SEXAFS Data Analysis and Examples

Often a comparison of raw data directly yields useful structural information. An example is given in Figure 2, which shows SEXAFS spectra[8] above the palladium L_2 edge for 1.5 monolayers of Pd evaporated onto a Si (111) surface, along with pure Pd and the bulk compound Pd_2Si. It is clear just from looking at the spectra and without detailed analysis that the thin layer of Pd reacts to give a surface compound similar to the palladium silicide and completely different from the metallic Pd. By contrast, a thin layer of silver, studied in the same experiment, remains as a metallic Ag overlayer, as judged from its SEXAFS wiggles.

Fourier Transformation

One of the major advantages of SEXAFS over other surface structural techniques is that, provided that single scattering applies (see below), one can go directly from the experimental spectrum, via Fourier transformation, to a value for bond length. The Fourier transform gives a real space distribution with peaks in $|F(R)|$ at distances $R-\phi$. Addition of the phase shift, ϕ, then gives the true interatomic distance. Figure 3 shows how this method[9] is applied to obtain the O–Ni distance in the half-monolayer structure of oxygen absorbed on Ni (100). The data, after back-

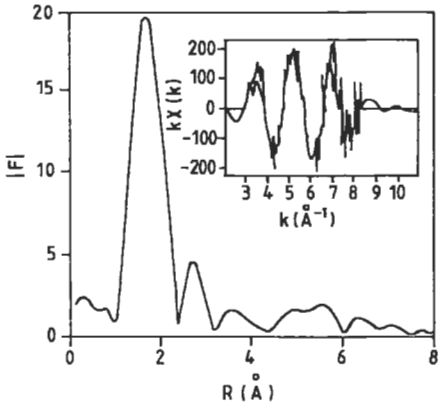

Figure 3 **The modulus of the Fourier transform of the SEXAFS spectrum for the half-monolayer coverage on Ni(100) The SEXAFS spectrum itself is shown in the inset with the background removed.**

ground subtraction, yield a Fourier transform dominated by a single peak at $R \approx$ 1.73 Å. Correcting for the phase shift derived from bulk NiO, a nearest neighbor distance of $R_{O-Ni} \approx 1.98$ Å is obtained.

Fourier transforms cannot be used if shells are too close together, the minimum separation ΔR being set by the energy range above the absorption edge over which data are taken, typically ≈0.2 Å for SEXAFS. A useful application of the Fourier technique is to filter high-frequency noise from a spectrum. This is done by putting a window around a peak in R-space and transforming back into k-space: each shell may be filtered and analyzed separately, although answers should always be checked against the original unfiltered spectrum.

Curve Fitting

The beauty of using photons is that their absorption is easily understood and exactly calculable, so that structural analysis can be based on comparisons of experimental data and calculated spectra. Statistical confidence limits can easily be computed, although the systematic errors will often be much greater than the random errors. An example of data analysis by curve fitting is depicted in Figure 4 for the system of ⅔ monolayer of Cl on Ag (111).[10] The nearest neighbor Cl–Ag (2.70 Å) and Cl–Cl (2.89 Å) shells are so close in distance that they cannot be separated in a Fourier transform approach, but they are easily detected here by the fact that their atomic backscattering factors vary differently with energy, thus influencing the overall shape of the spectrum.

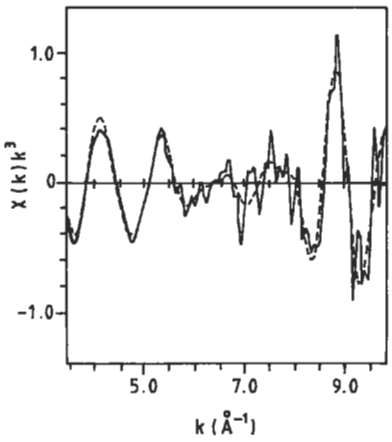

Figure 4 **The EXAFS function $\chi(k)$, weighted by k^3, experimental data for ⅓ monolayer of Cl on Ag(111) (solid line), with the best theoretical fit (dashed line) from the least-squares curve fitting method with neighbors as distances of 2.70 Å (Ag), 2.89 Å (CL), 3.95 Å (Ag) and 5.00 Å (Cl).**

Complications

The simple theory assumes single scattering only, in which electrons go out only from the absorber atom to a backscatterer and back, rather than undertaking a journey involving two or more scattering atoms. Such multiple scattering may sometimes be important in EXAFS, especially when atoms are close to collinear, giving wrong distances and coordination numbers. With modern, exact theories of EXAFS one can deal with multiple scattering, but it is complicated and time-consuming, and a unique analysis may be impossible. However, nearest neighbor information can never be affected by multiple scattering, since there is no possible electron path shorter than the direct single scattering route.

EXAFS analysis usually assumes a shell of neighbors at a certain distance, with a Gaussian (normal) distribution around that distance to cope with the effects of disorder, both static (positional) and dynamic (vibrational). Static disorder arises where, even at zero temperature, a range of sites is occupied, as found particularly with amorphous or glassy samples. EXAFS samples directly the distance between nearby atoms and thus measures correlated motion, giving a disorder (Debye–Waller) factor smaller than that derived from long-range diffraction techniques like XRD or LEED. Vibrational amplitudes at a surface usually differ from those in the bulk, and SEXAFS spectra measured at different angles have been used to reveal surface dynamics, resolving vibrations parallel and perpendicular to a single-crystal surface.

The assumption of harmonic vibrations and a Gaussian distribution of neighbors is not always valid. Anharmonic vibrations can lead to an incorrect determination of distance, with an apparent mean distance that is shorter than the real value. Measurements should preferably be carried out at low temperatures, and ideally at a range of temperatures, to check for anharmonicity. Model compounds should be measured at the same temperature as the unknown system. It is possible to obtain the real, non-Gaussian, distribution of neighbors from EXAFS, but a model for the distribution is needed[11] and inevitably more parameters are introduced.

Some of these complications can lead to an incorrect structural analysis. For instance, it can be difficult to tell whether one's sample has many nearest neighbors with large disorder or fewer neighbors more tightly defined. Analysis routines are available at almost all synchrotron radiation centers: curve fitting may be the best method because most of the factors affecting the spectrum vary with energy in a different way and this k-dependence allows them to be separated out. A curved-wave computational scheme can be especially useful for analyzing data closer to the absorption edge.

NEXAFS Data Analysis and Examples

Chemical Shifts and Pre-Edge Features

The absorption edge occurs when the photon energy is equal to the binding energy of an electron core level. Shifts in the position of the edge are caused by small differences in the chemical environment, as in ESCA (XPS). If one needs to know the exact energy of the edge, perhaps for comparison with other published data, then a model compound with a calibrated energy should be measured under the same conditions as the unknown. Features may be seen before the absorption edge, most obviously in transition metals and their compounds. These small peaks are characteristic of local coordination (octahedral, tetrahedral or whatever); their intensity increases with oxidation state.

Atomic Adsorbates

The NEXAFS region near an absorption edge is usually discarded in an EXAFS analysis because the strong scattering and longer mean free path of the excited photoelectron give rise to sizable multiple-scattering corrections. For several atomic adsorbates NEXAFS has been modeled by complicated calculations, which show that scattering involving around 30 atoms, to a distance >5.0 Å from the absorbing atom, contributes to the spectrum. This makes interpretation difficult and not useful for practical purposes, except possibly for fingerprinting different adsorption states.

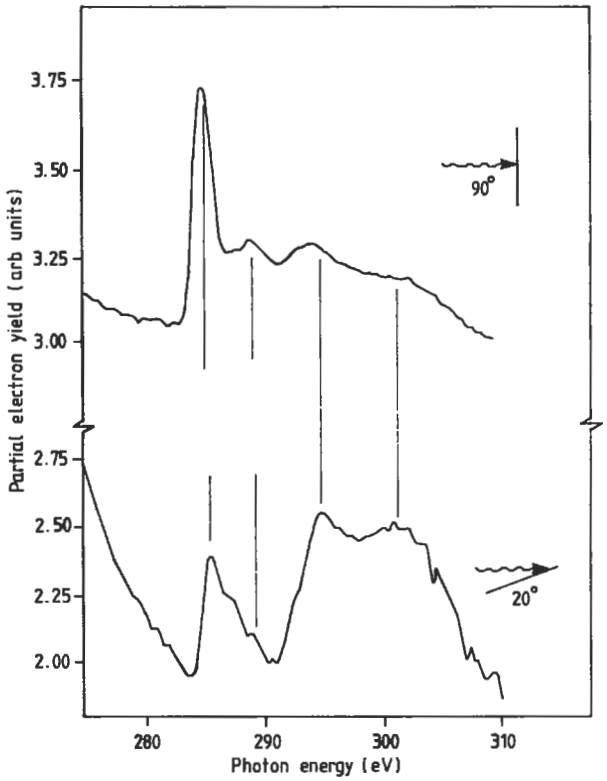

Figure 5 **NEXAFS spectra above the C K-edge for a saturation coverage of pyridine C_5H_5N on Pt(111), measured at two different polarisation angles with the X-ray beam at normal incidence and at 20° to the sample surface.**

Molecular Adsorbates—Orientation

For molecules, NEXAFS often contains intense resonances that dwarf the effects of atomic scattering in the spectrum. These resonances arise from states that are localized in space within the molecule, rather than being spread out and shared between various atoms: they are thus mainly characteristic of the molecule itself and only weakly affected by differences in the way the molecule may be bonded to the surface. Despite the technical difficulties, most NEXAFS work has been done at the carbon K-edge. An example is depicted in Figure 5, which shows NEXAFS for a saturation coverage of pyridine C_5H_5N on Pt (111), measured at different angles to the photon beam.[12] Peak A is identified as a π resonance, arising from transitions from the C 1s state to the unfilled π^* molecular orbital. Peak B comes from CO impurity. Peaks C and D are transitions to σ shape resonances that lie in the plane of the molecule. The variation of intensity of the π and σ resonances with polarization angle gives the molecular orientation, each peak being maximized when the polarization vector E lies along the direction of the orbital. The π intensity is great-

est when **E** is parallel to the surface ($\theta = 90°$), so the π orbitals must lie parallel to the surface. Therefore the pyridine molecule must stand upright on the Pt (111) surface. NEXAFS alone tells us only the orientation with respect to the top plane of the substrate, not the detailed bonding to the individual atoms, nor which end of the molecule is next to the surface: this detailed geometry must be determined from other techniques.

There may be deviations from the perfect angular dependence due to partial polarization of the X rays or to a tilted molecule. This can be investigated by analysis of the intensities of the resonances as a function of angle. Measuring the intensity of NEXAFS peaks is not always straightforward, and one has to be careful in removing experimental artifacts from the spectrum and in subtracting the atomic absorption background, for which various models now exist. Detailed analysis is not always needed, for instance the mere observation of a π resonance can be chemically useful in distinguishing between π and di-σ bonding of ethylene on surfaces. NEXAFS can be applied to large molecules, such as polymers and Langmuir-Blodgett films. The spectra of polymers, such as those[13] depicted in Figure 6, contain a wealth of detail and it is beyond the current state of knowledge to assign all the peaks. However, the sharper, lower lying ones are attributed to π^* molecular orbital states. Changes in these features were observed after deposition of submonolayer amounts of chromium, from which it is deduced that the carbonyl groups on the polymers are the sites for initial interaction with the metal overlayer. It has been suggested[4] that most examples of molecular adsorbate NEXAFS may be analyzed with quite simple models that decompose complex molecules into building blocks of diatoms or rings.

Intramolecular Bond Length

The energies of shape resonances often seem inversely related to the intramolecular bond length, with a long bond giving a σ resonance close to threshold and a shorter bond showing a peak at higher energy.[4] This effect has been demonstrated for many small molecules, although some do not fit the general trend. A mathematical relationship has been derived to allow estimates of bond length, but with the current state of knowledge it seems safest to restrict its use to diatomic molecules or ligands. With this procedure, intramolecular chemisorption bond lengths can be determined to an accuracy of ± 0.05 Å.

Conclusions

X-ray absorption spectroscopy is an important part of the armory of techniques for examining pure and applied problems in surface physics and chemistry. The basic physical principles are well understood, and the experimental methods and data analysis have advanced to sophisticated levels, allowing difficult problems to be solved. For some scientists the inconvenience of having to visit synchrotron radia-

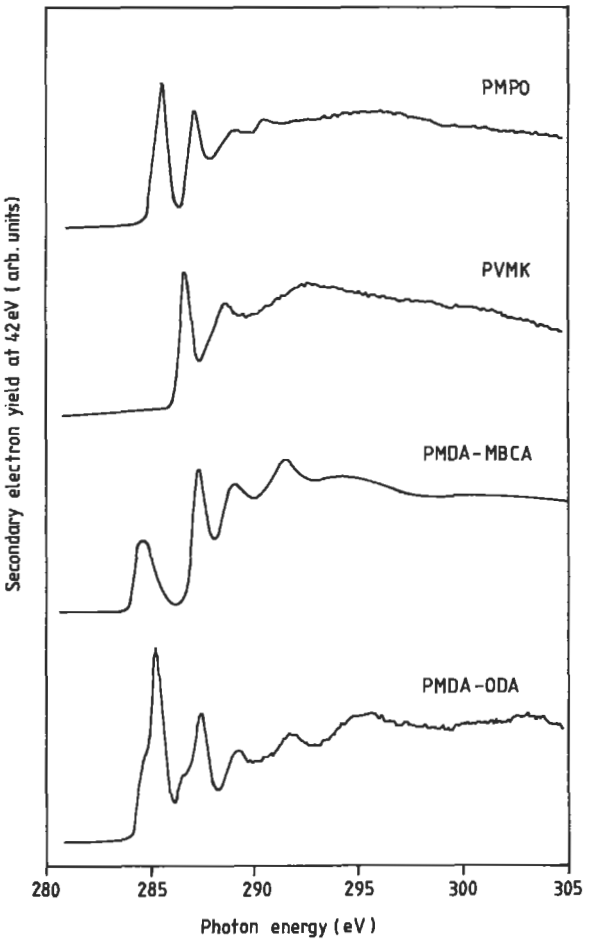

Figure 6 **NEXAFS spectra above the C K-edge for the polymers PMPO poly (dimethyl phenylene oxide), PVMK poly (vinyl methyl ketone), PMDA-MBCA PI poly (pyromellitimido 4, 4-methylene bis-cyclohexyl amine) and PMDA-ODA PI poly (pyromellitimido oxydianiline).**

tion centers is outweighed by the unique surface structural information obtainable from SEXAFS/NEXAFS. Nevertheless, although they are powerful techniques in the hands of specialists, it is difficult to foresee their routine use as analytical tools.

A database of model compound spectra and a better understanding of complex molecules would help the inexperienced practitioner. More dilute species could be studied by brighter synchrotron radiation sources. An obvious experimental improvement would be to use a polychromatic energy-dispersive arrangement for speedier data collection. In such a scheme the X rays are dispersed across a sample so that photons having a range of energies strike the specimen, and a detection

method has to be used that preserves the spatial distribution of the emitted electrons. Currently available photon fluxes are such that collection times less than or about one second should then be obtainable for a NEXAFS spectrum.

Related Articles in the Encyclopedia

AES, EXAFS, LEED/RHEED, XPS, and XRF

References

1 D. Norman. *J. Phys. C: Solid State Phys.* **19,** 3273, 1986. Reprinted with an appendix bringing it up to date in 1990 as pp. 197–242 in *Current Topics in Condensed Matter Spectroscopy.* Adam Hilger, 1990. An extensive review of SEXAFS and NEXAFS, concentrating on physical principles.

2 P. H. Citrin. *J. Phys. Coll.* **C8,** 437, 1986. Reviews all SEXAFS work up to 1986, with personal comments by the author.

3 *X-Ray Absorption: Principles, Applications, Techniques of EXAFS, SEXAFS and XANES.* (D.C. Koningsberger and R. Prins, Eds.) Wiley, New York, 1988. The best book on the subject. Especially relevant is the chapter by J. Stöhr, which is a comprehensive and readable review of SEXAFS.

4 J. Stöhr. *NEXAFS Spectroscopy.* Springer-Verlag, New York, 1992. A book reviewing everything about NEXAFS.

5 D. Norman. In *Physical Methods of Chemistry.* Wiley–Interscience, New York, in press. Practical guide with emphasis on chemical applications.

6 *The X-Ray Data Booklet.* Lawrence Berkeley Laboratory, Berkeley, is an excellent source of information.

7 M. de Crescenzi. *Surf. Sci.* **162,** 838, 1985.

8 J. Stöhr and R. Jaeger. *J. Vac. Sci. Technol.* **21,** 619, 1982.

9 L. Wenzel, D. Arvanitis, W. Daum, H. H. Rotermund, J. Stöhr, K. Baberschke, and H. Ibach. *Phys. Rev. B.* **36,** 7689, 1987.

10 G. M. Lamble, R. S. Brooks, S. Ferrer, D. A. King, and D. Norman. *Phys. Rev. B.* **34,** 2975, 1986.

11 T. M. Hayes and J. B. Boyce. *Solid State Phys.* **37,** 173, 1982. Good background reading on EXAFS.

12 A. L. Johnson, E. L. Muetterties, and J. Stöhr. *J. Chem. Soc.* **105,** 7183, 1983.

13 J. L. Jordan-Sweet, C. A. Kovac, M. J. Goldberg, and J. F. Morar. *J. Chem. Phys.* **89,** 2482, 1988.

4.4 XPD and AED

X-Ray Photoelectron and Auger Electron Diffraction

BRENT D. HERMSMEIER

Contents

Introduction

X-ray Photoelectron Diffraction (XPD) and Auger Electron Diffraction (AED) are well-established techniques for obtaining structural information on chemically specific species in the surface regions of solids. Historically, the first XPD effects were observed in single crystals some 20 years ago by Siegbahn et al.[1] and Fadley and Bergstrom.[2] A short time later, others[3] began to quantify the technique as a surface and surface–adsorbate structural tool and, more recently, Egelhoff[4] applied AED to metal-on-metal systems to determine growth modes and shallow interface structures, which has strongly influenced the current expansion to materials research. In general, these pioneering studies have introduced XPD and AED to areas like adsorbate site symmetry, overlayer growth modes, surface structural quality, and element depth distributions,[5, 6] any one of which may be a key to understanding the chemistry or physics behind a measured response. Studies as widely separated as the initial stages of metallic corrosion, interface behavior in epitaxial thin films, and semiconductor surface segregation have already profited from XPD and AED experiments. A broad range of research communities—catalysis, semiconductor,

corrosion, material science, magnetic thin film, and packaging, stand to benefit from these diffraction studies, since surfaces and interfaces govern many important interactions of interest. XPD and AED are used primarily as research tools, but, given the hundreds of XPS and AES systems already in use by the aforementioned research communities, their move to more applied areas is certain.

Adaptation of existing XPS and AES instruments into XPD and AED instruments is straightforward for spectrometers that are equipped with an angle resolved analyzer. Traditionally, XPD and AED instruments were developed by individuals to address their specific questions and to test the limits of the technique itself. Today, surface science instrument companies are beginning to market XPD and AED capabilities as part of their multi-technique spectroscopic systems. This approach has great potential for solving both a broad range of problems as is typically found in industrial laboratories and in studies that intensely focus on atomic details, as ins often found in university laboratories. Key to obtaining quality results, whichever the mode of operation, are in the speed of data acquisition, the angular and energy resolution, the accessible angular range, and the capability to meaningfully manipulate the data.

The reader is urged to review the XPS and AES articles in this Encyclopedia to obtain an adequate introduction to these techniques, since XPD and AED are actually their by-products. In principle two additions to XPS and AES are needed to perform diffraction studies, an automated two-axis sample goniometer and an angle-resolved analyzer. Ultrahigh-vacuum conditions are necessary to maintain surface cleanliness. Standard surface cleaning capabilities such as specimen heating and Ar^+ sputtering, usually followed by sample annealing, are often needed. Sample size is rarely an issue, especially in AED where the analysis area may be as small as 300 Å, using electron field emitter sources.

Excellent reviews of XPD and AED have been published by Fadley[5, 6] and are strongly recommended for readers needing information beyond that delineated here.

Basic Principles

The diffraction mechanisms in XPD and AED are virtually identical; this section will focus on only one of these techniques, with the understanding that any conclusions drawn apply equally to both methods, except where stated otherwise. XPD will be the technique discussed, given some of the advantages it has over AED, such as reduced sample degradation for ionic and organic materials, quantification of chemical states and, for conditions usually encountered at synchrotron radiation facilities, its dependence on the polarization of the X rays. For more details on the excitation process the reader is urged to review the relevant articles in the Encyclopedia and appropriate references in Fadley.[5, 6]

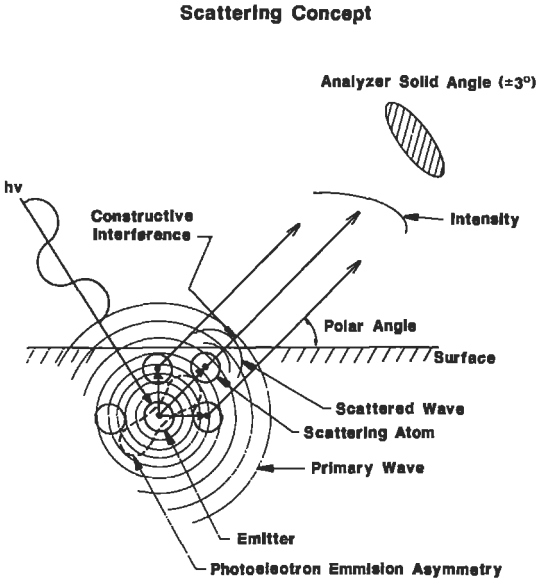

Figure 1 **Simplistic schematic illustration of the scattering mechanism upon which X-ray photoelectron diffraction (XPD) is based. An intensity increase is expected in the forward scattering direction, where the scattered and primary waves constructively interfere.**

XPD is a photoelectron scattering process that begins with the emission of a spherical electron wave created by the absorption of a photon at a given site. This site selectivity allows XPD to focus on specific elements or even on different chemical states of the same element when acquiring diffraction data. The excitation process obeys dipole selection rules, which under special conditions may be used to enhance regions or directions of interest by taking advantage of photoelectron emission asymmetries in the emission process; for example, enhanced surface or bulk sensitivity can be obtained by aligning the light's electric field vector to be parallel or perpendicular to the sample's surface plane, respectively. This flexibility, unfortunately, is not available in most spectrometers because the angle between the excitation source and the analyzer is fixed. The spherical photoelectron wave propagates from the emitter, scatters off neighboring atoms, and decays in amplitude as $1/r$. The scattering events modify the photoelectron intensity reaching the detector relative to that of the unscattered portion, or primary wave. A physical picture of this is given in Figure 1, where a spherical wave propagating outward from the emitter passes through a scattering potential to produce a spherically scattered wave that is nearly in phase with the primary wave in the forward direction. Since the primary and scattered waves have only a slight phase shift in this direction the two waves can be thought of as constructively interfering. However, since both waves

are spherical and have different origins, they will tend to interfere destructively in off-forward directions. This interference process results in increased intensity for emission geometries in which rows of closely spaced atoms become aligned with the entrance axis to the analyzer.

The diffraction pattern itself is simply the mapping of the intensity variations as a function of polar or azimuthal angles. Angular scans can be obtained by rotating the sample while leaving the analyzer fixed, or by rotating the analyzer and leaving the sample fixed. In either case, an intensity profile is obtained for a given core-level transition. The recipe is therefore quite simple. First, to determine whether the sample is structurally ordered, one simply looks for any intensity variation as a function of angle; if found it can be concluded that there exists some kind of order over the probing length of the photoelectron. Second, to identify a low-index crystallographic direction, one looks for maxima along various logical or predetermined directions, such as those associated with cleavage planes or previously identified by X-ray diffraction. Usually this confirmation can be done by directly monitoring the intensity with a ratemeter if the specimen is reasonably well ordered. Third, to determine the symmetry of the structure, often the main goal in XPD, one collects several polar and azimuthal scans to correlate the appearance of diffraction peaks at measured angles to suspected Bravais lattice structures having near-neighbor atoms at similar angles. Fourth, one monitors changes in the diffraction features as a function, for example, of sample temperature or of overlayer thickness. This is particularly informative when comparing absorbate or overlayer symmetries with that of the substrate in a fingerprint analysis mode. Although the intensities are dominated by forward scattering processes, a detailed understanding must consider contributions to the detected intensity by all of the scattering atoms within several lattice constants of the emitter. To simulate such a scattering process, a kinematical or single-scattering approach is sufficient if the electron's kinetic energy is greater than 150 eV, and if it is not necessary to fully understand the fine structure in the diffraction pattern.[5, 6] Complicated multiple-scattering calculations can also aid in the quantification of XPD data by more accurately addressing intensity anisotropies and improving identification of the fine structure. But more often than not, multiple-scattering effects contribute little to the basic understanding of the structure, and thus will not be discussed further. Single-scattering results will be displayed along with experimental data, and compared to geometric arguments for resemblance.

Unlike more common electron diffraction methods, such as LEED and RHEED, XPD is dominated by near-neighbor interactions averaged over a very short time scale. The $1/r$ decay of a spherical wave, coupled with a short mean free path for electrons in solids (due to inelastic scattering energy losses), uniquely allows XPD to probe the local, or short-range, order about an emitter. This is simplified further by the incredibly short times involved in the scattering process. Only 10^{-17} seconds are required for a photoelectron to experience a scattering event

while typical crystal fluctuations, which can average out short-range order effects, occur on a much longer time scale. In essence, the scattering events can be thought of as a snapshot of the local crystal order.

A brief comment needs to made to clear up some misleading information that has entered the literature concerning the scattering mechanism upon which XPD and AED are based. Frank et al.[7] have proposed what they believe to be a new technique capable of solving surface structure problems. The technique, which they have termed angular distribution Auger microscopy (ADAM), is based on an argument claiming that emitted Auger electrons are solid particles that are blocked by neighboring atoms in the solid. This interpretation is in direct contradiction with the scattering picture presented in the basic principles section which is based on the quantum mechanical wave nature of electrons, a picture for which there is overwhelming evidence from theoretical and experimental comparisons. In light of this, no further consideration will be given to ADAM in this article.

Experimental Details

The specimen to be studied usually will be an ordered solid, such as a single crystal or a textured sample, that is rigidly mounted face-up on the goniometer. Prior knowledge of the crystal orientation is greatly beneficial. In most instances the samples or substrates are aligned with a low-index direction normal to the surface by means of standard X-ray diffraction methods, e.g., by back-reflection Laue or θ–2θ scans. The surface plane of the sample should lie in, or as close as possible to, the polar rotation axis; the maximum offset should be 2.5 mm. An often more critical alignment is that needed to get the surface normal and the azimuthal rotation axis to coincide. This will minimize crystal "wobble," thus minimizing ambiguous diffraction effects (usually apparent as a sloping background) that are accentuated at grazing emission angles, where signal intensities are dominated by an instrumental function highly responsive to slight changes in polar angle. Proper azimuthal alignment is obtained by centering a surface-reflected laser beam to within $\pm$ 0.25° during azimuthal rotation. Polar rotation should have a range of at least 120° to include both grazing and surface-normal emissions directions and the azimuthal range should have a minimum of 200°, preferably 380°, to allow for the full rotational symmetry.

Since diffraction data is angle dependent, an angle-resolved analyzer is necessary to discriminate electron trajectories, allowing only those electrons with similar emission directions to reach the detector. The practical upper limit for the acceptance solid-angle is approximately $\pm$ 12°, with $\pm$ 3° being a more common value. (There have been some high angular-resolution studies done at $\pm$ 1.5° showing diffraction fine structure that led to a more quantitative description of the observed structure, however this will not be necessary for routine structure determinations.) Increasing the angular resolution is usually a straightforward task that involves the

physical placement of an aperture or an array of cylinders in front of the electron-analyzing optics. Or, if an electron lens is included, voltage adjustments to the lens elements may act to effectively reduce the acceptance solid angle. This, as an example, has been done by the author on a VG MICROLAB II spectrometer, which has a two-element lens. Here, when the front elements are powered and the back elements are grounded, a ± 12° solid angle results, while a ± 4° solid angle may be achieved by powering the back elements and grounding the front. In either mode, the implementation of a reduced solid angle and sample rotation is a relatively easy and inexpensive procedure, and may be accomplished with many existing electron spectrometers.

Illustrative Examples

Surface adsorbates

From environmental to packaging to catalysis issues, the need to understand how molecules interact chemically and bond to a surface is paramount. XPD is an extremely good candidate for investigating adsorbate–substrate interactions because chemical shifts in the core-level transitions can lead to the identification of a specific species, and the scattering of core-level photoelectrons can lead to the determination of the structure in which they exist. Consider the initial interaction of gaseous CO on room temperature Fe (001).[8] At this temperature Fe (001) has a bcc lattice structure with a fourfold symmetric surface. At a coverage of less than a monolayer, it was known that the CO adsorbs to the Fe, residing in fourfold hollow sites with only the C making direct contact with the Fe. The orientation of the C-O bond remained a question. It was proposed that this early stage of CO coverage on Fe (001) produced an intermediary state for the dissociation of the C and O, since that the CO bond was tilted with respect to the surface normal, unlike the upright orientation that CO was found to possess on Ni.[5] Although near-edge X-ray adsorption fine structure (NEXAFS) results measured a tilt in the CO bond, the results were not very quantitative regarding the exact angle of the tilt. XPD, on the other hand, gave the CO bond angle as 35 ± 2° relative to the surface, as determined from the large forward scattering peak depicted in by the solid line Figure 2a along the (100) azimuth. Here the ordinate is plotted as the C 1s intensity divided by the O 1s intensity. Plotting this ratio effectively removes instrumental contributions to the diffraction pattern, the oxygen atoms have no atoms above them from which their photoelectrons can scatter and thus should be featureless. The azimuthal scan shown in Figure 2b was taken at a polar angle of 35° to enhance the C 1s diffraction signal. From the fourfold symmetry and knowledge of the crystallographic orientation of the Fe, it is clear that the tilt direction lies in the <100> planes, as depicted in Figure 2c; the absence of a diffraction peak in the [1$\bar{1}$0] polar scan shown by the dashed line in Figure 2a helps to confirm this.

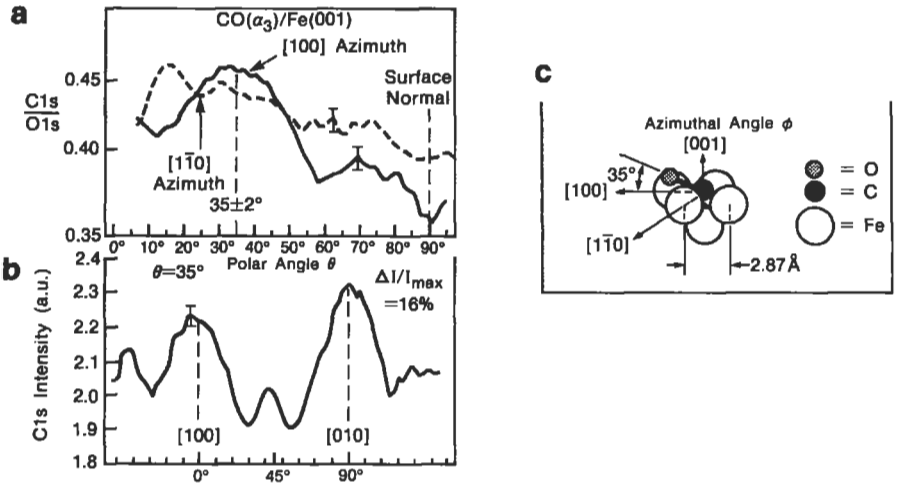

Figure 2 **Experimental data from an early stage of CO adsorbed on Fe (001) known as the α_3 state: polar scans (a) of the C 1s–O 1s intensity ratio taken in two Fe (001) azimuthal planes, the (100) and the (1$\bar{1}$0) (the C 1s and O 1s electron kinetic energies are 1202 eV and 955 eV, respectively); C 1s azimuthal scan (b) taken at the polar angle of maximum intensity in (a); and geometry (c) deduced from the data.**

The intensity anisotropies in Figure 2b associated with the <100> diffraction peaks are similar in magnitude. This was found to be true also for the other two quadrants not shown here and suggests that there is no preferred tilt of the CO molecule into any one of the four quadrants. This also demonstrates the high level of sensitivity one can expect for an XPD pattern, considering that less than a quarter monolayer of (low-Z) CO molecules, i.e., only those with C–O bonds pointing in the direction presented in Figure 2b, contribute to a 16% anisotropy. To put this into perspective, a "perfect" single crystal will yield an anisotropy of about 50%. Since the diffraction features are dominated by near-neighbor scattering events, a 16% intensity change is not too surprising and further suggests that even though the CO molecules are tilted along four different directions they are highly ordered along each of them. This presents some practical experimental assurance of the sensitivity that can be expected from XPD or AED.

Overlayers

Perhaps the best examples to illustrate the analysis strength of XPD and AED are the epitaxial growth modes of deposited overlayers. Here, the structure and chemistry of an overlayer, or the new interface, will influence the properties of the film. To control such effects, an understanding of the basic structure and chemistry is essential. Epitaxial Cu on Ni (001) is an excellent example for demonstrating the

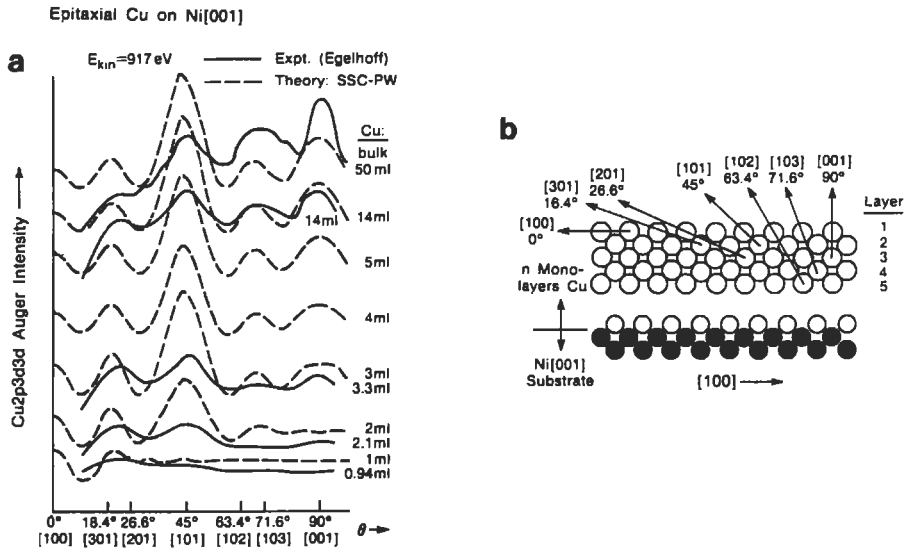

Figure 3 **Experimental and calculated results (a) for epitaxial Cu on Ni (001). The solid lines represent experimental data at the Cu coverage indicated and the dashed lines represent single-scattering cluster calculations assuming a plane wave final state for the Cu *LMM* Auger electron; A schematic representation (b) of the Ni (010) plane with 1–5 monolayers of Cu on top. The arrows indicate directions in which forward scattering events should produce diffraction peaks in (a).**

types of structural information that can be obtained for a metal-on-metal system. Figure 3a shows several experimental polar diffraction patterns obtained using the Cu *LMM* Auger transition, which are compared to single-scattering cluster calculations that use plane waves to represent the emitted electrons.[9] XPD patterns using the Cu $^2P_{3/2}$ core level would look virtually identical. Figure 3b gives a diagrammatic sketch to help interpret the origins of the diffraction features. The diagram should be viewed, layer by layer, from the top down; the angles associated with each arrow, when in full view, indicate the directions in which a diffraction peak should appear. For example, after the second monolayer is formed three arrows are in full view, at angles of 0°, 18°, and 45°. The first arrow represents an emission direction in which it is physically impossible to collect data. The other two arrows appear in the experimental data of Figure 3a only after a second monolayer is deposited. The appearance of these diffraction peaks with the deposition of the second monolayer is consistent with intensity maxima occurring along directions having neighboring atoms. This is then confirmed by the sudden appearance of the diffraction peak at 90° after the deposition of the third layer.

Although the interpretation presented is conceptually inviting, caution must be taken not to extend it beyond what is reliable. For this reason, results from single-scattering cluster calculations are included in Figure 3. By calculating the intensity from a fabricated atomic cluster, in which atoms can be removed from the cluster at will, a very accurate understanding of the relative contributions for various atoms can be made. Indeed, the peaks at 45° and 90° result almost entirely from scattering events with the near-neighbor atoms along these directions, whereas the peak at 70° gets its intensity not only from the atoms along this direction but, to some degree, also from the near-neighbor atoms at 90° and 45°. One should be careful when attributing diffraction intensities to atoms in the solid that are more than a few neighbors away.

Polar XPD data taken in a low-index azimuthal plane creates the opportunity to directly obtain the c/a axis ratio for measuring induced lattice strain. This has been done by Chambers et al.[10] for the Cu–Ni system mentioned above and, more recently, by the author et al.[10] for thin Co layers in a Co–Pt superlattice. The induced strain in the overlayer alters the angles, excluding the 90° peak, at which the diffraction signals appear. The change in angle leads to a direct determination of the type and degree of strain present in the sample.

Special Topics

As is common to most techniques, XPD and AED have spawned related techniques that are too specialized to present in detail here, but the reader should be at least aware of some of the more interesting ones, which show future possibilities.

Holography

It is the goal of XPD and AED to give chemically specific structural information in ordered samples. The presentation of such data has recently been simplified from angular plots to real space images. The mechanics of the data collection procedure remains the same as in normal XPD or AED, with the additional need to acquire data over the full hemisphere of angular space above the surface, or a significant fraction thereof. The difference emerges in the final treatment, which involves a Helmholtz-Kirchoff Fourier transformation. The result is an image that apparently allows one to display the surface structure from numerous perspectives and to directly measure the bond distances in the solid.[11] It is important to point out, however, that using the preceding scattering theories one can get exactly the same information, minus the friendly display.

Spin-Polarized Photoelectron Diffraction

This article has been devoted to understanding the structural order at surfaces and interfaces through XPD and AED. However, these techniques are not limited to

structural studies. An example can be found in studies of surface magnetic ordering. Here XPD is thought to offer a unique approach by taking advantage of the physics involved in the emission of outer core-level photoelectrons from magnetic atoms and in the electron-atom scattering process. Simply put, such photoelectrons will have multiple final states separated in energy (several eV) and spin. An energy-dispersive analyzer can thus be used to monitor spin-polarized signals. The scattering process consisting of two contributions, nonmagnetic (Coulombic) and magnetic (exchange), will affect a spin-parallel photoelectron differently from an antiparallel one. It will thus give rise to spin-polarized XPD or spin-polarized photoelectron diffraction (SPPD).[12] The simplest approach for understanding SPPD is to monitor spin-split photoelectron peaks as a function of crystal temperature, as opposed to angle (as done in XPD). A relative change in intensity, beyond that expected by lattice responses to the temperature (such as Debye-Waller effects) can be attributed to a change in the magnetic order of the solid. As has been observed, a sudden change occurs in the relative photoelectron intensities at temperatures well above the bulk ordering temperature that is speculated to be a surface short-range ordering temperature. As a final point, since the spin-polarized beam of photoelectrons is referenced internally to the sample and not the spectrometer, as in numerous other spin-polarized electron experiments, it appears to be able to measure antiferromagnetic as well as ferromagnetic materials.

Surface Melting

The ability of XPD and AED to measure the short-range order of materials on a very short time scale opens the door for surface order–disorder transition studies, such as the surface solid-to-"liquid" transition temperature, as has already been done for Pb and Ge. In the case of bulk Ge,[13] a melting temperature of 1210 K was found. While monitoring core-level XPD photoelectron azimuthal scans as a function of increasing temperature, the surface was found to show an order–disorder temperature 160° below that of the bulk.

Valence Bands

The ambiguous nature of valence band peaks are well known, especially when further complicated by having a multicomponent system, such as compounds and alloys. XPD has been used to offer unique insight in addressing this problem. The process is straightforward. By directly comparing the degree of similarity between core-level diffraction patterns and diffraction patterns of deconvolved valence band peaks, one can immediately determine which peaks are due to which elements.[14] From here, the total density of states can be separated then into its partial densities of states. This has important implications, as the use of valence-band regions for identifying complicated compounds increases.

Conclusions

There is a clear need in materials science to achieve a more quantitative understanding of chemical and structural properties of surfaces and interfaces. XPD and AED offer both with a relatively small investment in time and equipment, if one is using XPS or AES already. With a foundation in spectroscopy, XPD and AED are well suited for elemental analysis; XPD is capable even of giving quantitative chemical state information in many cases. Once the element or elements are identified, information on structure can be gathered. The approach emphasized in this article is the simplest and most straightforward, and consists of correlating the main experimental diffraction peaks obtained from several diffraction scans with near-neighbor atomic positions, leading to a determination of the lattice type. When an overlayer is deposited onto a substrate, there is the unique ability to obtain diffraction patterns from both simultaneously—measuring the quality of the lattice matching as well as the structure. As a further step, exact atomic positions can be obtained by comparing the experimental diffraction data with scattering theory. The information gained for a given amount of effort is substantial.

Hundreds of electron spectrometers are already being used to pursue surface chemical information, many on crystalline and textured materials, and it seems only reasonable that a number of these could benefit further from the addition of structural analysis capabilities. Should this addition be realized, one would expect that XPD and AED will move more from the basic research environments into applied areas. An example of this can be seen with the future growth of thin-film technology where XPD and AED may serve a valuable function in quality control issues by monitoring the degree of surface texturing or interface diffusion. Whatever the future may be, surface structure and chemistry will inevitably play a key role in materials research. XPD and AED are good candidates for doing both.

Related Articles in the Encyclopedia

XPS, AES, EXAFS, SEXAFS, LEED, RHEED.

References

1 K. Siegbahn, U. Gelius, H. Siegbahn, and E. Olsen. *Phys. Lett.* **32A,** 221, 1970.

2 C. S. Fadley and S. A. L. Bergstrom. *Phys. Lett.* **35A,** 375, 1971.

3 S. Kono, C. S. Fadley, N. F. T. Hall and Z. Hussein. *Phys. Rev. Lett.* **41,** 117,1978; S. D. Kevan, D. H. Rosenblatt, D. Denley, B.-C. Lu, and D. A. Shirley. *Phys. Rev. Lett.* 41,1565 (1978); D. P. Woodruff, D. Norman, B. W. Holland, N. V. Smith, H. H. Farrell and M. M. Traum. *Phys. Rev. Lett.* **41,** 1130, 1978.

4 W. F. Egelhoff. *Phys. Rev.* **B30,** 1052, 1984; R. A. Armstrong and W. E. Egelhoff. *Surf. Sci.* **154,** L225, 1985.

5 C. S. Fadley. *Prog. Surf. Sci.* **16,** 275, 1984; C. S. Fadley. *Physica Scripta.* **T17,** 39, 1987. In this and the following reference, the author gives a detailed overview of XPD and AED, including a quantitative description of the scattering theory behind the diffraction effect, instrumental considerations, and comparisons with related techniques like extended X-ray absorption fine structure (EXAFS) and low-energy electron diffraction (LEED). Reference 6, especially, has a comprehensive profile on recent XPD and AED experiments that have strongly contributed to the field.

6 C. S. Fadley. in *Synchrotron Radiation Research: Advances in Surface Science* (R. Z. Bachrach, ed.) Plenum Press, New York, 1989.

7 D. G. Frank, N. Batina, T. Golden, F. Lu, and A. T. Hubbard. *Science.* **247,** 182, 1990.

8 R. S. Saiki, G. S. Herman, M. Yamada, J. Osterwalder, and C. S. Fadley. *Phys. Rev. Lett.* **63,** 283, 1989.

9 W. F. Egelhoff. *Phys. Rev.* **B30,** 1052, 1984; E. L. Bullock and C. S. Fadley. *Phys. Rev.* **B31,** 1212 (1985).

10 S. C. Chambers, H. W. Chen, I. M. Vitomirov, S. B. Anderson, and J. H. Weaver. *Phys. Rev.* **B33,** 8810, 1986; B. Hermsmeier, R. F. C. Farrow, C. H. Lee, E. E. Marinero, C. J. Lin, R. F. Marks, and C. J. Chien. *J. Magn. Mat.* 1990, in press.

11 G. R. Harp, D. K. Saldin, and B. P. Tonner. *Phys. Rev.* **B42,** 9199, 1990.

12 B. Hermsmeier, J. Osterwalder, D. J. Friedman, B. Sinkovic, T. Tran, and C. S. Fadley. *Phys. Rev.* **B42,** 11895, 1990.

13 U. Breuer, O. Knauff, and H. P. Bonzel. *J. Vac. Sci. Technol.* **A8,** 2489, 1989; D. J. Friedman, T. Tran, and C. S. Fadley. *The Structure of Surfaces* (S. Y. Tong, M. A. Van Hove, X. Xide, and K. Takayanagi, eds.) Springer-Verlag, Berlin, in press.

14 A. Stuck, J. Osterwalder, T. Greber, S. Hüfner, and L. Schlapbach. *Phys. Rev. Lett.* **65,** 3029, 1990.

4.5 LEED

Low-Energy Electron Diffraction

MAX G. LAGALLY

Contents

Introduction

Low-energy electron diffraction (LEED) is a technique for investigating the crystallography of surfaces and overlayers or films adsorbed on surfaces. LEED is generally performed with electron energies of 10–1000 eV. The limited penetration of electrons in this energy range provides the sensitivity to the surface. Diffraction of electrons occurs because of the periodic arrangement of atoms in the surface. This periodic arrangement can be conceptualized as parallel rows of atoms analogous to grating lines in a diffraction grating. Thus, diffraction in LEED occurs from rows of atoms, just as in its three-dimensional (3D) counterpart, X-ray diffraction, which can be considered as occurring from planes. The diffracted beams emanate from the crystal surface in directions satisfying interference conditions from these rows of atoms. The diffraction pattern and the intensity distribution in the diffracted beams can provide information on the positions of atoms in the surface and on the existence of various kinds of crystallographic disorder in the periodic arrangement of surface atoms.[1–7] In its most elementary form, LEED can be used to test for the existence of overlayer phases having a two-dimensional (2D) crystal

structure different from the surface on which they are adsorbed and to test whether a surface phase is ordered or disordered.

Although LEED is the best-known and most widely used surface crystallographic technique, other diffraction techniques can provide information on the surface structure. Because of its convenient configuration, reflection high-energy electron diffraction (RHEED) is used widely in the epitaxial growth of films. X-ray diffraction can also be used for surface crystallography under appropriate conditions. Thermal-energy atom diffraction (TEAS) is a powerful technique for looking at disorder on surfaces because of the high sensitivity of low-energy atoms to isolated surface atoms. Surface extended absorption fine structure (SEXAFS) and photoelectron (XPD) diffraction are specialized techniques that also can give structural information on surfaces. RHEED, XRD, XPD, and SEXAFS are covered in separate articles.

Basic Principles

Surface Crystallography Vocabulary

If an imaginary plane is drawn somewhere through a perfectly periodic 3D crystal, and the two halves of the crystal are separated along this plane, ideal surfaces are formed. If the imaginary plane corresponds to an (*hkl*) plane in the bulk crystal, the surface is defined as an (*hkl*) surface, using the usual Miller indices. The periodic arrangement of atoms in the surface can be viewed as a 2D lattice; that is, every point in this arrangement can be reached by a translation vector. The smallest translation vectors define the unit mesh, the 2D analog of the unit cell. Primitive unit meshes contain one lattice point per mesh; nonprimitive meshes, more than one lattice point per mesh. Figure 1a shows the five 2D Bravais nets. The unit mesh vectors are conventionally defined, as shown, with the angle between the unit vectors $\geq 90°$, **a** denoting the shorter unit vector, and **b** (aligned horizontally) the longer one. A 2D lattice may also have a basis. The lattice is defined by those points that can be reached by a translation vector. The basis is the conformation of atoms around each of these points.

The arrangement of lattice points in a 2D lattice can be visualized as sets of parallel rows. The orientation of these rows can be defined by 2D Miller indices (*hk* see Figure 1b). Inter-row distances can be expressed in terms of 2D Miller indices, analogous to the notation for 3D crystals.

In the discussion so far, an ideal termination of the bulk crystal has been assumed at the surface; that is, the positions of atoms in the surface have been assumed to be the same as what they would have been in the bulk before the surface was created. This may not be true. Reconstruction, a rearrangement of atoms in the surface and near-surface layers, occurs frequently. It is caused by an attempt of the surface to lower its free energy by eliminating broken bonds. The atomic layers par-

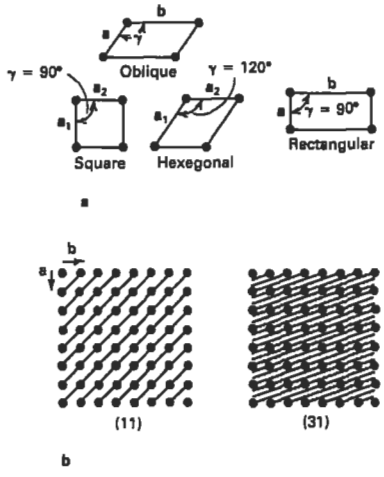

Figure 1 **Unit meshes and 2D Miller indices. (a) Examples of 2D Bravais nets; (b) examples of families of rows with Miller indices referenced to the unit mesh vectors. (11) and (31) families of rows are shown.**

ticipating in this reconstruction can be considered as a different phase having a different periodic arrangement of atoms. Even when no reconstruction occurs, adsorption of a foreign species onto the substrate surface from the ambient gas, from a deliberately created beam of atoms, or as a consequence of segregation of an impurity out of the bulk creates a surface phase termed an overlayer. An overlayer can be a fraction of a single atomic layer or several atom layers forming a thin film. The overlayer phase has its own crystal structure, which may or may not be related in a simple manner to that of the substrate surface. Examples are shown in Figure 2. An overlayer may be commensurate or incommensurate with the substrate. Commensurate overlayers have unit meshes that are related by simple rational numbers to those of the substrates on which they are adsorbed. Incommensurate layers do not. The unit mesh of overlayers is defined as a multiple of that unit mesh of the substrate surface that would be produced by the ideal termination of the bulk lattice. Thus, (100) and (111) surfaces of an fcc crystal have square- and parallelogram-shaped primitive unit meshes, respectively (Figure 1a), both of which would be considered (1 × 1) unit meshes. Commensurate overlayer unit meshes are then p($m \times n$) or c($m \times n$) (Figures 2a and 2b, respectively), where p and c refer to primitive and centered overlayer unit meshes relative to the primitive substrate unit mesh, and m and n are constants. An example of a complete unit mesh description of an overlayer on a particular substrate is W(110) p(2 × 1) O, which describes an oxygen overlayer adsorbed on the (110) surface of tungsten having a unit mesh twice that of the primitive W(110) unit mesh in the **a** direction and the same as the W(110) unit mesh in the **b** direction.

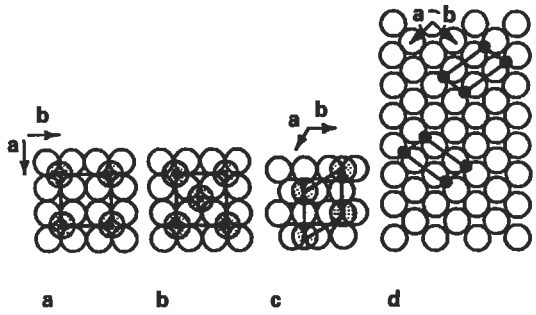

Figure 2 **Examples of overlayer structures with appropriate notation. (a) fcc (100) p(2 × 2); (b) fcc (100) c(2 × 2); (c) fcc (111) p($\sqrt{3} \times \sqrt{3}$)R30°; (d) bcc (110) p(2 × 1) and bcc (110) p(1 × 2). The two orientations for the unit mesh in (d) are both possible because of the symmetry of the substrate; they have the same free energy and are called degenerate.**

The overlayer unit mesh is sometimes rotated relative to that of the substrate (Figure 2c). An example of the notation for such a structure is Ni (111) ($\sqrt{3} \times \sqrt{3}$) R30° O, which describes an oxygen overlayer on Ni (111) whose unit mesh is $\sqrt{3}$ times as large as the substrate mesh in both unit mesh directions and is rotated by 30° relative to the substrate mesh. The symmetry of the substrate is often low, permitting the formation of energetically equivalent structures rotated relative to each other or translated by some specific amount, as shown in Figure 2d. Domains having symmetry related structure are called rotational or translational *antiphase domains* and are degenerate; that is, they have the same free energy, and there is no preference for the formation of one over the other. Overlayers with ($m \times n$) meshes generally also form ($n \times m$) meshes; for example, p(2 × 1) → p(1 × 2) and c(2 × 4) → c(4 × 2) (Figure 2d). Most low-symmetry surfaces allow degenerate overlayer or reconstruction domains.

Diffraction From Surfaces

Diffraction from surfaces can be viewed most simply as the scattering of waves from families of lattice rows that connect scattering centers lying in a single plane (Figure 3). If a wave with wavelength λ is permitted to fall at an angle of incidence θ_0 onto a family of rows separated from each other by a distance d_{hk}, the 2D Laue condition can be calculated for constructive interference between incoming and outgoing waves by considering the difference in paths traveled by the rays striking two adjacent rows of atoms:

$$m\lambda = d_{hk}(\sin\theta_{mhmk} - \sin\theta_0) \tag{1}$$

where the difference in paths traveled by two adjacent rays is m wavelengths. The wavelength λ of electrons (in Å) is related to their energy E (given in eV) by

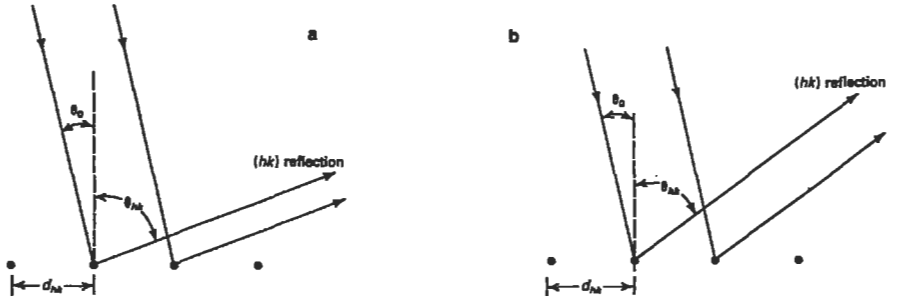

Figure 3 **Diffraction from a family of rows spaced d_{hk} apart and its dependence on wavelength. Each solid circle represents a row of atoms in the plane of the paper. Rays with wavelength λ fall on this family of rows at an angle θ_0. Interference maxima occur at angles θ_0 that satisfy Equation (2). Only the first-order reflection is shown. (a) Longer wavelength; (b) shorter wavelength.**

$$\lambda = \sqrt{\frac{150}{E}} \tag{2}$$

For a fixed incident-beam energy, that is, a fixed wavelength, and a fixed angle of incidence, each family of (*hk*) rows diffracts radiation at the appropriate exit angle, θ_{hk}. If a fluorescent screen or other detector is positioned to intercept these scattered beams, a diffraction pattern having the symmetry of the surface or overlayer unit mesh will be observed (Figure 4). At the center of the pattern will be the (00) beam, which has a path difference of zero and is therefore not sensitive to d_{hk}, that is, to the relative lateral positions of the surface atoms. Around it will be the first-order diffracted beams ($m = 1$) from each family of possible rows that can be drawn through the surface atoms, for example, (10), (01), (11), (21), and so on. In addition, there will be higher-order reflections ($m \geq 1$) at larger angles. For example, the (20) and (30) reflections will fall on the extension of a line connecting the (00) and (10) beams; the (00), (11), (22), (33), etc., beams will be collinear, and so forth. Diffracted beams are indexed with the (*hk*) notation of the families of rows from which they are diffracted. Thus, the (10) beam is scattered from (10) rows in the direction perpendicular to these rows. The distance of the (*hk*) reflection from the mirror reflection, the (00) beam, is inversely related to the (*hk*) inter-row distance d_{hk}; see Equation (1).

If the energy of the incident beam or the angle of incidence is changed, the diffraction angles θ_{hk} adjust to continue to satisfy the Laue conditions. For example, if the energy is increased, the entire pattern will appear to shrink around the (00) beam because θ_{hk} becomes smaller.

Any periodicity in the surface or overlayer different from that of the clean unreconstructed surface produces additional diffracted beams. A unit mesh larger than

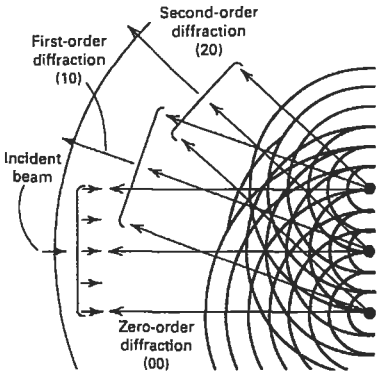

Figure 4 **Interference pattern created when regularly spaced atoms scatter an incident plane wave. A spherical wave emanates from each atom; diffracted beams form at the directions of constructive interference between these waves. The mirror reflection—the (00) beam—and the first- and second-order diffracted beams are shown.**

that of the substrate surface yields diffracted beams that are nearer each other; i.e., if d_{hk} is larger, θ_{hk} is smaller; see Equation (1).

The diffraction conditions can be depicted most easily using a reciprocal-lattice and Ewald construction (Figure 5).[4] The Ewald sphere provides a schematic description of the conservation of energy; that is, since diffraction involves elastic scattering, the incident and exiting beams have the same energy. Its radius is inversely proportional to the wavelength λ. The reciprocal lattice for a single layer of atoms consisting of families of rows is a set of rods (hk) normal to the crystal surface having spacing $2\pi/d_{hk}$. The intersection of the Ewald sphere and the reciprocal-lattice rods is a graphical solution of the Laue equation, Equation (1), and therefore yields the diffraction pattern. As the energy of the incident beam or the angle of incidence is varied, the radius of the Ewald sphere or its orientation relative to the rods changes, consequently also changing the points of intersection with the rods. The directions of the outgoing vectors define the directions of the diffracted beams.

The discussion of diffraction so far has made no reference to the size of the 2D "grating." It has been assumed that the grating is infinite. In analogy with optical or X-ray diffraction, finite sizes of the ordered regions on the surface (finite-sized gratings) broaden the diffracted beams. From an analysis of the diffracted-beam shapes, the types of structural disorder in the surface region can be identified and quantified.[7–9]

Surface sensitivity in LEED is provided by the limited mean free path for inelastic scattering of slow electrons. This mean free path is the distance traveled by an electron in the solid before it collides inelastically, loses energy, and thus becomes

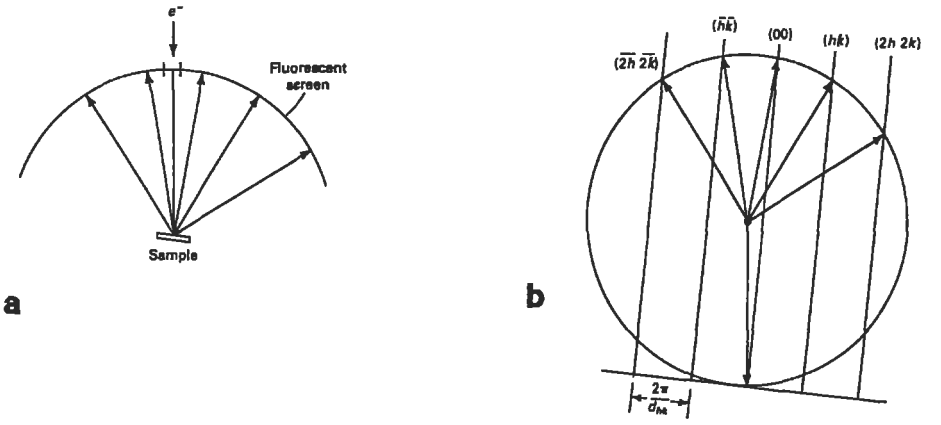

Figure 5 **Reciprocal-lattice and Ewald construction corresponding to LEED and comparison to real-space picture. (a) Real-space schematic diagram of diffraction from a surface. The electron beam is incident on the sample along the direction given by e^-. The five diffracted beams represent the $(\overline{2h}\ \overline{2k})$, $(\overline{hk})$, (00), (hk), and $(2h\ 2k)$ beams from a family of rows (hk) with spacing d_{hk}. (b) The corresponding cut through the reciprocal-lattice and the Ewald construction. The reciprocal-lattice rods are normal to the crystal surface, given by the nearly horizontal line. They represent the same set of beams as in (a). The Ewald sphere always intersects the origin of the reciprocal lattice at the point of incidence of the incoming ray. Directions of the diffracted beams depend on the radius $(2\pi/\lambda)$ of the Ewald sphere. Similarly, as the orientation of the crystal surface is changed in relation to the incident beam, the reciprocal lattice rotates about its origin.**

lost for diffraction. The mean free path in the energy range of LEED is from 4 to 20 Å. Because a layer spacing is of the order of 3 Å, these slow electrons probe only a few atomic layers. The inelastic scattering of slow electrons is discussed further in other articles, e.g., AES and XPS.

Diffraction Measurements

Figure 6 shows a schematic diagram of a typical LEED system.[10] The electron gun can produce a monoenergetic beam of approximately 10–1000 eV, with beam sizes typically a fraction of a mm, but ranging in newer instruments down to ~10 μm. The goniometer generally allows two sample motions— rocking about an axis in the plane of the crystal surface and rotation about an axis normal to the crystal surface—as well as heating and sometimes cooling of the sample and temperature measurement capability. The detector consists usually of concentric grids and a fluorescent screen. The grids filter inelastically scattered electrons that also emanate

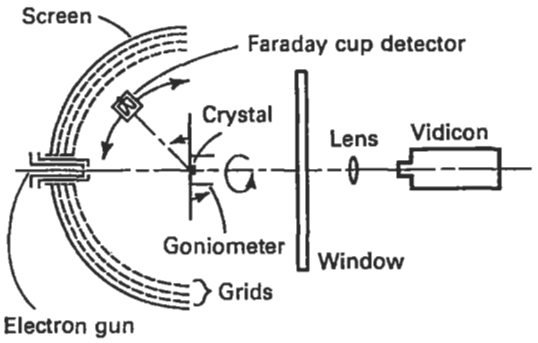

Figure 6 **LEED diffractometer. The vidicon camera can be interfaced with a computer to record the diffraction pattern displayed on the fluorescent screen. The Faraday collector may contain a channeltron electron multiplier for added sensitivity.**

from the crystal surface. For accurate measurement of beam currents and beam profiles a Faraday cup detector can be used. The Faraday cup is biased to exclude inelastically scattered electrons. Modern detectors incorporate a channeltron electron multiplier or a resistive anode encoder in the detector, depending on the need for sensitivity or resolution.[10]

The simplest diffraction measurement is the determination of the surface or overlayer unit mesh size and shape. This can be performed by inspection of the diffraction pattern at any energy of the incident beam (see Figure 4). The determination is simplest if the electron beam is incident normal to the surface, because the symmetry of the pattern is then preserved. The diffraction pattern determines only the size and shape of the unit mesh. The positions of atoms in the surface cannot be determined from visual inspection of the diffraction pattern, but must be obtained from an analysis of the intensities of the diffracted beams. Generally, the intensity in a diffracted beam is measured as a function of the incident-beam energy at several diffraction geometries. These "intensity-versus-energy" curves are then compared to model calculations.[6]

Diffraction is useful whenever there is a distinct phase relationship between scattering units. The greater the order, the better defined are the diffraction features. For example, the reciprocal lattice of a 3D crystal is a set of points, because three Laue conditions have to be exactly satisfied. The diffraction pattern is a set of sharp spots. If disorder is introduced into the structure, the spots broaden and weaken. Two-dimensional structures give diffraction "rods," because only two Laue conditions have to be satisfied. The diffraction pattern is again a set of sharp spots, because the Ewald sphere cuts these rods at precise places. Disorder in the plane broadens the rods and, hence, the diffraction spots in x and y. The existence of streaks, broad spots, and additional diffuse intensity in the pattern is a common

occurrence indicating that the overlayer or surface structure is not perfect. The angular profile of diffracted beams provides information on disorder and finite-size effects in surfaces analogous to particle size broadening in X-ray diffraction of bulk materials. The measurement of LEED angular profiles as a function of diffraction parameters, such as energy, angles, and beam order, makes it possible to distinguish types of surface disorder, including finite island sizes, strain, crystal mosaic, monatomic and multiatomic steps at the surface, and regular or irregular domain or antiphase boundaries.[7–9] To measure a profile, a detector with a narrow slit or a point aperture must be used to minimize the influence of instrumental broadening.[10]

Examples of Uses

Surface-sensitive diffraction require a high vacuum because surface contamination rates from ambient gases are rapid. Contaminated surfaces are generally disordered and generally do not provide diffraction patterns. Because the beam penetration is so small, even a few layers of adsorbed gas or oxide can mask the underlying pattern. The ideal surface preparation method is cleavage in vacuum. Cleavage exposes an internal interface that has not been subjected to ambient atmospheric contamination. However, cleavage is limited to a few crystals and generally to only one surface orientation of these crystals. Samples not cleaved in vacuum must be cut from a single crystal, polished, and oriented carefully to the desired surface using a Laue diffraction camera. Standard polishing procedures are used.

LEED can be used to determine the atomic structure of surfaces, surface structural disorder, and to some extent, surface morphology, as well as changes in structure with time, temperature, and externally controlled conditions like deposition or chemical reaction. Some examples are briefly discussed here:

1 Surface order and cleanliness. The most common use of LEED is in association with other surface analysis or surface research methods, to check surface structural order and cleanliness. A visual display of the diffraction pattern is used. An expected pattern, with sharp diffracted beams, is an indication that the surface is clean and well ordered.

2 Surface atomic structure. The integrated intensity of several diffracted beams is measured as a function of electron beam energy for different angles of incidence. The measurements are fitted with a model calculation that includes multiple scattering. The atomic coordinates of the surface atoms are extracted.[6] (See also the article on EXAFS.)

3 Step density. For surfaces containing steps, both the step height and step density can be determined by measuring the angular profile of diffracted beams (the shape of the beam in angle) at specific conditions of energy and angle. This measurement can be static or dynamic, the latter if the surface is evolving with

time, as a function of temperature or adatom coverage. The analysis is straightforward in terms of kinematic theory.[7–9] Similar measurements can identify surface strain, the existence of structural domains or islands, and crystal mosaic.[7] (For crystal mosaic see also the article on XRD.)

4 Phase transitions in overlayers or surfaces. The structure of surface layers may undergo a transition with temperature or coverage. Observation of changes in the diffraction pattern gives a qualitative analysis of a phase transition. Measurement of the intensity and the shape of the profile gives a quantitative analysis of phase boundaries and the influence of finite sizes on the transition.[7]

5 Dynamics of phase transitions, ordering, disordering, and growth. Measurement of the time evolution of the diffracted intensity and the shape of diffracted beams gives information on the kinetic mechanisms of ordering and disordering, growth laws, and finite-size effects.[9] Transitions from layered to cluster growth, as well as transitions from amorphous to crystalline phases, can be investigated. Activation energies for diffusion and domain boundary motion can, in principle, be extracted.

6 Thermal properties of overlayer atoms. Measurement of the intensity of any diffracted beam with temperature and its angular profile can be interpreted in terms of a surface-atom Debye–Waller factor and phonon scattering.[4] Mean-square vibrational amplitudes of surface atoms can be extracted. The measurement must be made away from the parameter space at which phase transitions occur.

7 Chemical reactions of surfaces. Diffraction can be used qualitatively to identify different surface phases resulting from adsorption and chemical reaction at surfaces.[3] Reaction rates can be investigated by following the evolution of diffracted beam intensities.

8 Grain size in textured films. For films having a preferred growth direction—e.g., (111)—LEED can be used to determine the preferred direction and the grain size parallel to the surface. The preferred direction is obtained from the symmetry of the diffraction patterns, while the grain size is obtained from the shape in angle of diffracted beams.

Limitations of LEED

Surface-sensitive diffraction is, for the most part, restricted to analysis of surfaces of single crystals and overlayers and films on such surfaces. If a polycrystalline sample is illuminated using a beam of low-energy electrons, each crystallite surface exposed will create its own diffraction pattern, all of which will be superimposed on the fluorescent screen detector. If more than a few orientations are illuminated by the beam, the pattern becomes too complicated to analyze. However, if the size of the

LEED beam is reduced to less than the sample grain size, individual grains in a polycrystal can be investigated. It is difficult to make low-energy electron beams this small, but in some materials large grain sizes can be achieved in polycrystals.

Because electrons are charged, only materials having reasonable conductivity can be investigated. Insulators and ceramics pose difficulties because charge accumulates on the sample and eventually prevents the incident beam from striking the surface. Most insulators can be investigated with special techniques, such as providing surface conduction paths near the analysis area or using very thin samples mounted on a conducting plate.

The use of LEED for quantitative determinations of atomic positions in surfaces is complicated by the multiple scattering of the electrons, a process that is highly sensitive to scattering geometry. An accurate goniometer and detection scheme are required to measure intensities for which the scattering geometry is precisely known. A detector with high sensitivity is required to measure the frequently small intensities in this type of measurement, but high resolution is not necessary. Massive calculations that include multiple scattering are necessary to fit data to extract atomic positions.

Measurements of surface disorder require a high resolving power (the ability to distinguish two close-lying points in the diffraction pattern). Quantitative measurements of surface disorder are limited in the following manner: the worse the resolving power, the smaller the maximum scale of surface disorder that can be detected. For example, if the maximum resolvable distance of the diffractometer is 100 Å, then a surface that has steps spaced more than 100 Å apart will look perfect to the instrument. The theoretical analysis of disorder is much simpler than that for atomic positions.

Conclusions

LEED is the most powerful, most widely used, and most developed technique for the investigation of periodic surface structures. It is a standard tool in the surface analysis of single-crystal surfaces. It is used very commonly as a method to check surface order. The evolution of the technique is toward greater use to investigate surface disorder. Progress in atomic-structure determination is focused on improving calculations for complex molecular surface structures.

Preparation of this article was supported by the National Science Foundation, Solid State Chemistry Program.

Related Articles in the Encyclopedia

RHEED, XRD, XPD, and EXAFS

References

1 J. J. Lander. *Prog. Solid State Chem.* **2,** 26, 1965.

2 P. J. Estrup. In *Modern Diffraction and Imaging Techniques in Materials Science.* (S. Amelinckx, R. Gevers, G. Remaut, and J. Van Landuyt, Eds.) North-Holland, 1970; and P. J. Estrup and E. G. McRae. *Surf. Sci.* **25,** 1, 1971.

3 G. A. Somorjai and H. H. Farrell. *Adv. Chem. Phys.* **20,** 215, 1972. Contains listings of overlayer phases that have been observed to that date.

4 M. B. Webb and M. G. Lagally. *Solid State Phys.* **28,** 301, 1973. A detailed discussion at a more advanced level.

5 G. Ertl and J. Küppers. *Low-Energy Electrons and Surface Chemistry.* Verlag Chemie, Weinheim, 1974, Chps. 9 and 10. An introductory treatment of diffraction.

6 J. B. Pendry. *Low-Energy Electron Diffraction.* Academic Press, New York, 1974. Theoretical treatment, principally on surface atomic structure determination.

7 M. G. Lagally. In *Methods of Experimental Physics—Surfaces.* (R. L. Park and M. G. Lagally, Eds.) Academic Press, New York, 1985, Vol. 22, Chp. 5.

8 M. Henzler. *Top. Curr. Phys.* **4,** 117, 1977. Basic information on use of LEED to analyze steps and step disorder on surfaces.

9 M. G. Lagally. In *Reflection High-Energy Electron Diffraction and Reflection Electron Imaging of Surfaces.* (P. K. Larsen and P. J. Dobson, Eds.) Plenum, New York, 1989.

10 M. G. Lagally and J. A. Martin. *Rev Sci. Instr.* **54,** 1273,1983. A review of LEED instrumentation.

4.6 RHEED

Reflection High-Energy Electron Diffraction

DONALD E. SAVAGE

Contents

Introduction

Reflection High-Energy Electron Diffraction (RHEED) is a technique for probing the surface structures of solids in ultrahigh vacuum (UHV). Since it is a diffraction-based technique, it is sensitive to order in solids and is ideally suited for the study of clean, well-ordered single-crystal surfaces. In special cases it can be used to study clean polycrystalline samples as well. It gives essentially no information on the structure of amorphous surfaces, which makes it unsuitable for use on sputter-cleaned samples or in conjunction with sputter depth profiling, unless the sample can be recrystallized by annealing.

The area of a surface sampled in RHEED is determined by the primary beam size at the specimen. The typical electron gun used for RHEED focuses the electrons to a spot on the order of 0.2 mm in diameter. The diffraction pattern should be interpreted as arising from a spatial average over an area whose width is the beam diameter and whose length is the beam diameter divided by the sine of the incidence angle. Of course, high-energy electrons can be focused to a much smaller spot, on the order of several Å. The detection of a RHEED feature as an electron beam is rastered along the surface is the basis for Scanning Reflection Electron Microcopy (SREM). The surface sensitivity of RHEED comes from the strong interaction between electrons and matter. Electrons with RHEED energies and a

grazing angle of incidence will scatter elastically from only the first few atomic layers. One disadvantage of using electrons is that the sample must be sufficiently conducting so as not to build up charge and deflect the primary beam. Also, electron-sensitive materials can be damaged during a measurement.

When used to examine a crystal surface, RHEED gives information on the surface crystal structure, the surface orientation, and the degree of surface roughness. Evidence for surface reconstruction (the rearrangement of surface atoms to minimize the surface energy) is obtained directly. In addition, when RHEED is used to study film growth on crystalline surfaces, it gives information on the deposited material's growth mode (i.e., whether it grows layer-by-layer or as three-dimensional (3D) crystallites), the crystal structure, the film's orientation with respect to the substrate, and the growth rate for films that grow layer-by-layer. RHEED is particularly useful in studying structure changes dynamically, i.e., as function of temperature or time. Combined with its open geometry (the area normal to the surface will have a direct line of sight to deposition sources) this feature makes it one of the most commonly used techniques for monitoring structural changes during molecular beam epitaxy (MBE).

Other diffraction techniques whose principles are similar to RHEED include Low-Energy Electron Diffraction (LEED), Thermal-Energy Atom Scattering (TEAS), and X-ray Diffraction. Of these, LEED is the most similar to RHEED, differing mainly by its normal-incidence scattering geometry. Atom scattering differs from RHEED in that it is more surface sensitive than electron diffraction because atoms scatter off the outer electronic shells of atoms in the surface. This makes TEAS very sensitive to defects like atomic steps, but corrugations due to the regular positions of atoms in the surface are difficult to observe. X-ray diffraction is the classic technique for measuring bulk crystal structure. With the use of high-brightness X-ray sources, the surface structure also can be determined by grazing incidence methods.

Basic Principles

The underlying principle of RHEED is that particles of matter have a wave character. This idea was postulated by de Broglie in (1924). He argued that since photons behave as particles, then particles should exhibit wavelike behavior as well. He predicted that a particle's wavelength is Planck's constant h divided by its momentum. The postulate was confirmed by Davisson and Germer's experiments in 1928, which demonstrated the diffraction of low-energy electrons from Ni.[2]

For nonrelativistic electrons, the wavelength (in Å) can be written

$$\lambda = \sqrt{\frac{150.4}{E}} \tag{1}$$

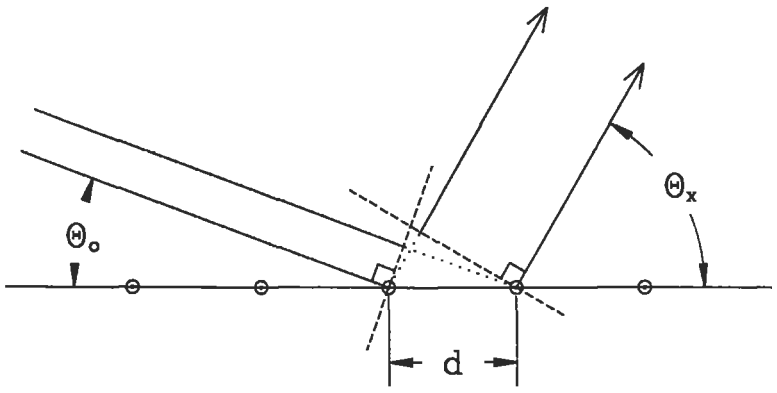

Figure 1 **Plane wave scattering from two consecutive lines of a one-dimensional diffraction grating. The wave scatters in-phase when the path difference (the difference in length of the two dotted sections) equals an integral number of wavelengths.**

where E is the energy of the electron (in electron volts). For a primary beam energy of 5–50 keV this relationship gives λ ranging from 0.17 to 0.055 Å.

Most of the features of a RHEED pattern can be understood qualitatively with the use of kinematic scattering theory, i.e., by considering the single scattering of plane waves off a collection of objects (in this case atoms). In the kinematic limit, the scattering of electrons from a single-crystal surface can be treated in the same way as the scattering of monochromatic photons from a two-dimensional (2D) diffraction grating. Given the wavelength and angle of incidence of the source radiation, the angles at which diffracted beams are scattered will depend on the grating line spacing (i.e., the atomic row spacing). Consider a plane wave of wavelength λ incident on a one-dimensional (1D) grating with line spacing d, as shown in Figure 1. The diffraction maxima occur when successive rays scatter in-phase, i.e., when their path difference is an integral number of wavelengths. The grating equation

$$n\lambda = d(\cos\theta_x - \cos\theta_0) \tag{2}$$

defines conditions where the maxima occur. Using Equation (2) one can show that to see higher order diffraction maxima when scattering from atomic rows, their relatively close spacing requires that the source wavelength be short.

The analogy of a crystal surface as a diffraction grating also suggests how surface defects can be probed. Recall that for a diffraction grating the width of a diffracted peak will decrease as the number of lines in the grating is increased.[3] This observation can be used in interpreting the shape of RHEED spots. Defects on a crystal surface can limit the number of atomic rows that scatter coherently, thereby broadening RHEED features.

In a diffraction experiment one observes the location and shapes of the diffracted beams (the diffraction pattern), which can be related to the real-space structure using kinematic diffraction theory.[4] Here, the theory is summarized as a set of rules relating the symmetry and the separation of diffracted beams to the symmetry and separation of the scatterers.

The location of a diffracted beam can be defined by specifying the magnitudes and the directions of the incoming and outgoing waves. This can be written in a shorthand notation using the momentum transfer vector **S**, where $\mathbf{S} = \mathbf{K}_{out} - \mathbf{K}_{in}$. The vector **K** is the wave propagation vector and has units of inverse length. Its magnitude is $2\pi/\lambda$, and it points along the direction of wave propagation. The vector **S** can be thought of as the change in momentum of a wave upon scattering. The periodicity of the scatterers will constrain the values of **S** where in-phase scattering occurs.

The dimensionality of the diffraction problem will have a strong effect on how the diffraction pattern appears. For example in a 1D problem, e.g., diffraction from a single line of atoms spaced d apart, only the component of **S** in the direction along the line is constrained. For a 2D problem, e.g., the one encountered in RHEED, two components of **S** in the plane of the surface are constrained. For a 3D problem, e.g., X-ray scattering from a bulk crystal, three components of **S** are constrained.

For a given structure, the values of **S** at which in-phase scattering occurs can be plotted; these values make up the reciprocal lattice. The separation of the diffraction maxima is inversely proportional to the separation of the scatterers. In one dimension, the reciprocal lattice is a series of planes, perpendicular to the line of scatterers, spaced $2\pi/d$ apart. In two dimensions, the lattice is a 2D array of infinite rods perpendicular to the 2D plane. The rod spacings are equal to $2\pi/$(atomic row spacings). In three dimensions, the lattice is a 3D lattice of points whose separation is inversely related to the separation of crystal planes.

Kinematic Diffraction from a 2D Plane

Electrons having energies and incident angles typical of RHEED can be treated as nearly nonpenetrating. As a result, atoms in the outermost plane are responsible for most of the scattering, and the resulting reciprocal lattice will be an array of rods perpendicular to the surface plane.

The symmetry and spacing of the 2D reciprocal-lattice mesh (the view looking down upon the array of reciprocal-lattice rods) will depend on the symmetry and spacing of atomic rows in the surface. Consider a crystal plane with lattice points located on the parallelogram shown in Figure 2a. The corresponding reciprocal mesh is shown in Figure 2b. One can construct this reciprocal-mesh by defining two nonorthogonal mesh vectors $\mathbf{A}^*$ and $\mathbf{B}^*$, whose lengths are equal to 2π divided by the separation between two adjacent atomic rows, and whose directions lie in the plane of the surface and are perpendicular to those rows. The (h, k) reciprocal-lattice rod is located by the vector $\mathbf{G}_{hk} = h\mathbf{A}^* + k\mathbf{B}^*$, where h and k are integers. Note

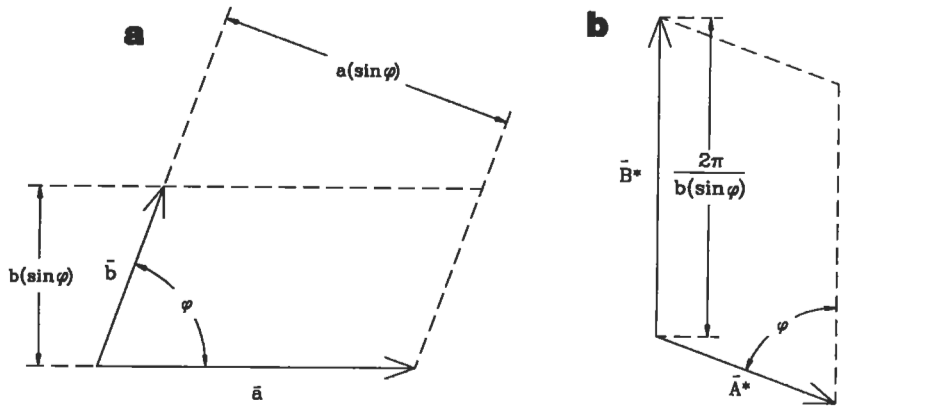

Figure 2 **View looking down on the real-space mesh (a) and the corresponding view of the reciprocal-space mesh (b) for a crystal plane with a nonrectangular lattice. The reciprocal-space mesh resembles the real-space mesh, but rotated 90°. Note that the magnitude of the reciprocal lattice vectors is inversely related to the spacing of atomic rows.**

that the symmetry of the surface reciprocal-mesh is the same as the symmetry of the surface lattice rotated by 90°. This result will always hold.

A diffraction pattern will be influenced strongly by the direction of the primary beam relative to the surface. The grazing angles used in RHEED can make the interpretation of the pattern difficult. For a specific choice of $\mathbf{K}_{in}$, i.e., primary beam energy and direction, the direction in which beams will be diffracted can be determined using the Ewald construction. This is a graphical construction that uses conservation of energy (for elastic scattering $|\mathbf{K}|$ is conserved) and momentum ($\mathbf{K}_{out}$ must lie on the reciprocal lattice). It is done by drawing $\mathbf{K}_{in}$ terminating at the origin of reciprocal-space. A sphere of radius $|\mathbf{K}|$ centered at the origin of $\mathbf{K}_{in}$ gives the locus of all possible scattered waves that conserve energy. The intersection of the sphere with the reciprocal-lattice locates the diffracted beams.

Consider as an example the RHEED pattern from GaAs (110). Gallium Arsenide can be cleaved along (110) planes; the resulting surface is nearly perfect. In Figure 3a the surface real-space lattice and the reciprocal-space mesh of GaAs (110) are shown. For GaAs (110), the surface real-space net is rectangular and has a 2-atom basis; only the lattice points (not the atom locations) are depicted. Figure 3b shows a portion of the Ewald construction for a primary beam incident along an azimuth parallel to the real-space lattice rows (spaced $|\mathbf{b}|$ apart), i.e., in the **a** direction, also called an [001] direction, and 20° from grazing. Note that the intersections of rows of reciprocal lattice rods with the Ewald sphere lie on circles similar to circles of constant latitude on a globe. If the diffracted beams are pro-

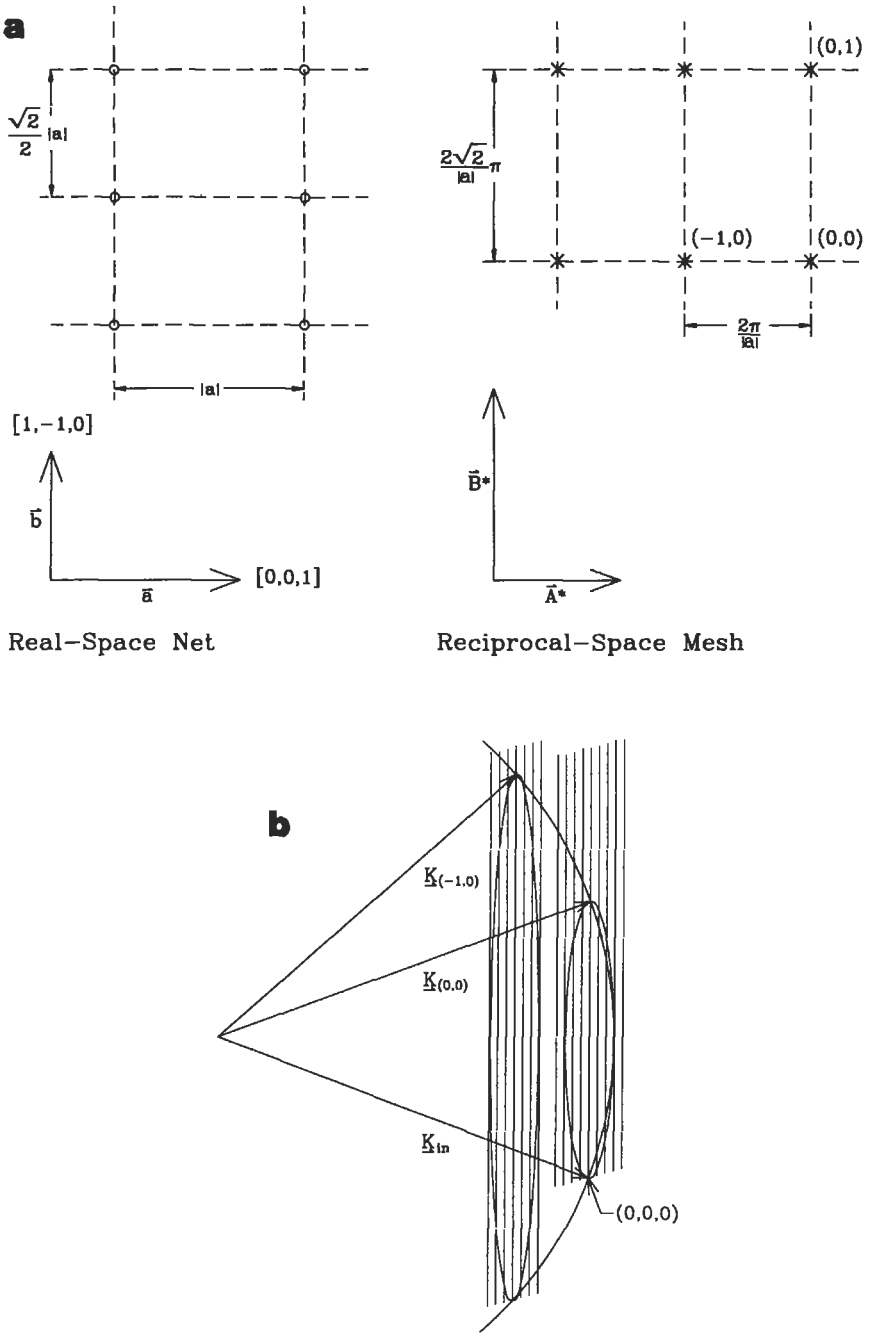

Figure 3 **(a) Real-space lattice and reciprocal-space mesh for the GaAs (110) plane. (b) Ewald construction for this surface with a primary beam incident along the a direction (the [001] azimuth) and elevated 20° from grazing.**

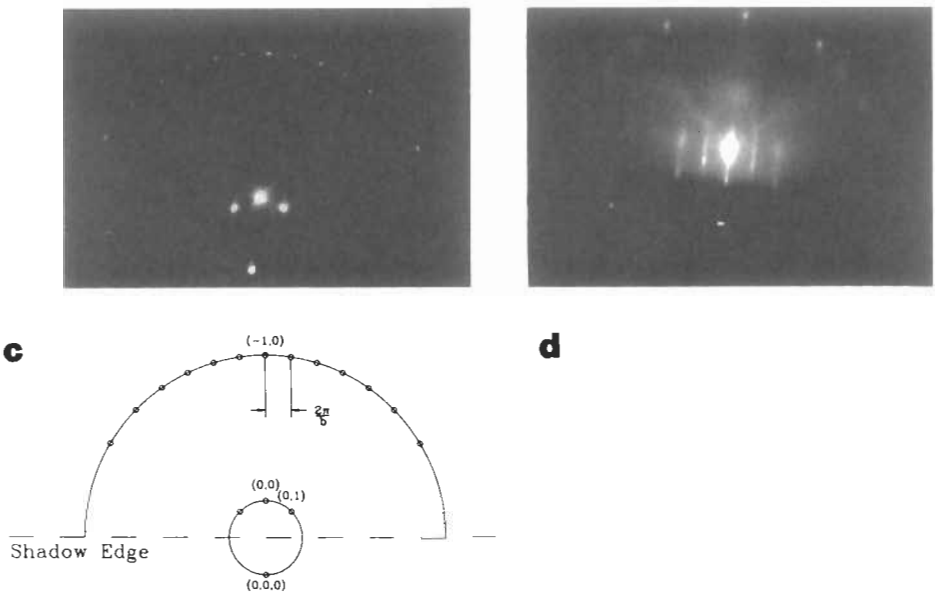

Figure 3 **(c) Photograph of a RHEED pattern from cleaved GaAs(110) obtained using a 10 KeV beam incident along the [001] azimuth at an angle of 2.4°—the spots lie along arcs (the inner is the 0th Laue circle, and the outer is the first Laue circle). The pattern is indexed in the drawing below the photo. (d) Photograph of the RHEED pattern after the sample has been sputter etched with 2-KeV Argon ions and subsequently annealed at 500° C for 10 minutes. The pattern is streaky, indicating the presence of atomic steps on the surface.**

jected forward onto a phosphor screen, they will appear as spots lying on semicircles in the same way that lines of constant latitude will inscribe circles if projected onto a screen located at the north pole of a globe. These rings are called Laue circles and are labeled 0, 1, etc., starting with the innermost. For this example, the 0th Laue zone contains the set of (0, k) reciprocal lattice rods. Note that if the crystal is rotated, thereby changing the orientation of primary beam azimuth so that it is no longer parallel to a set of rows, the projected diffracted beams will no longer lie on semicircles, and the diffraction pattern will appear skewed.

Figure 3c shows a photograph of a RHEED pattern from a cleaved GaAs (110) surface obtained with a 10-keV primary beam directed along an [001] azimuth. The diffracted maxima appear as spots lying along circles, as predicted, and are indexed in the view to the right. The diffracted spots of the 0th and 1st Laue circles are shown. One can tell from this view that the symmetry of the GaAs (110) surface net is orthogonal because the spots in the 1st Laue circle lie directly above those in the 0th. If the surface net had been a parallelogram, as in Figure 2b, the spots in the 1st Laue circle would be displaced. The spacing of the (0, k) rows is obtained from

the spacing of the spots on the Laue circle, and equals $2\pi/b$. The spacing of the (h, 0) rows (the lattice rows perpendicular to the [001] direction) can be obtained from the spacing between Laue circles, and equals $2\pi/a$. In practice, it is more common to rotate the sample until the primary beam is parallel to the (h, 0) atomic rows (for an orthogonal net, rotation by 90°) and to obtain the row spacing from the lateral spacing of the spots in that pattern. Some other the features to note in the pattern are the so-called transmitted beam, the shadow edge, and the specular reflection. The transmitted beam is the bright spot at the bottom of the photo. It arises when part of the incident beam misses the sample and strikes the phosphor screen directly. This is done intentionally by moving the sample partly out of the beam. The spot, also called the (000) beam, is a useful reference point because it locates the origin of reciprocal space. The spot directly above the transmitted spot is the specular reflection. Halfway between them is the shadow edge, below which no scattered electrons can reach the phosphor screen.

Figure 3d is a photograph of a cleaved GaAs (110) sample taken under conditions similar to Figure 3c but after the sample had been sputter etched with 2-keV Ar ions and subsequently annealed at 500° C for 10 minutes. Because the treatment resulted in a less intense diffraction pattern, the exposure time for this photograph was increased. This RHEED pattern shows streaks instead of spots, obscuring the location of the specular reflection. The separation of the streaks equals $2\pi/b$, as in the freshly cleaved surface, but the angular separation from circle to circle is no longer clear. The streaks arise because atomic steps are created during the sample treatment that limit the long-range order on the surface and broaden the reciprocal-lattice rods. Their intersections with the Ewald sphere produce the elongated streaks. Defects in the surface also give rise to a diffuse background intensity, making the shadow edge more visible. The effect of disorder on the diffraction pattern will be discussed more in the section on nonideal surfaces.

Applications

Surface Reconstruction

The size and symmetry of the surface lattice, which can differ from the bulk termination, is determined directly from the symmetry and spacing of beams in the diffraction pattern.[6] Because surface atoms have a smaller coordination number (i.e., fewer nearest neighbors) than bulk atoms they may move or rebond with their neighbors to lower the surface energy. If this occurs, the surface real-space lattice will become larger; i.e., one must move a longer distance on the surface before repeating the structure. As a result additional reflections, called superlattice reflections, appear at fractional spacings between integral-order reflections. One example of this is the (7×7) reconstruction of Si (111). The real-space lattice for this reconstructed surface is 7 times larger than the bulk termination. If the sample is well prepared, 6 fractional-order spots are observed between the integral-order spots on

a Laue circle and, more importantly, 6 fractional-order Laue circles are observed.[7] In MBE, one of the uses of RHEED is to monitor the surface reconstruction during deposition to obtain optimal growth conditions. An example is in the growth of GaAs on GaAs (100), where different reconstructions are observed depending on the surface stoichiometry. Deposition parameters can be varied to obtain the desired reconstruction.

Nonideal Surfaces

All real surfaces will contain defects of some kind. A crystalline surface must at the very least contain vacancies. In addition, atomic steps, facets, strain, and crystalline subgrain boundaries all can be present, and each will limit the long-range order on the surface. In practice, it is quite difficult to prepare an atomically flat surface.

Because defects limit the order on a surface, they will alter the diffraction pattern, primarily by broadening diffracted beams.[8] Methods have been developed, mostly in the LEED literature, to analyze the shape of diffracted beams to gain information on step distributions on surfaces. These methods apply equally well to RHEED.

A statement that one will find in the MBE literature is that a smooth surface will give a "streaky" RHEED pattern while a rough surface will give a "spotty" one. This is in apparent contradiction to our picture of an ideal RHEED pattern. These statements can be reconciled if the influence of defects is included. A spotty RHEED pattern that appears different from spots along a Laue circle will result from transmission of the primary beam through asperities rising above the plane of a rough surface. This type of pattern is described below. A flat surface, one without asperities but having a high density of defects that limit order within a plane, will give rise to a streaky RHEED pattern. If a smooth and flat surface is desired, a streaky pattern is preferable to a transmission pattern, but a surface giving a streaky pattern is not ideally flat or smooth.

Limiting long-range order within the plane of the surface will broaden the reciprocal lattice rods uniformly. For a plane with dimensions $L \times L$, the width of a rod will be approximately equal to $2\pi/L$. The streaking is caused by the grazing geometry of RHEED. The Ewald sphere will cut a rod at an angle such that the length is approximately $1/(\sin\theta_x)$ times the width, where θ_x is the angle the exit beam makes with the surface. For $\theta_x \sim 3°$, this is a factor of 20.

What gives rise to streaks in a RHEED pattern from a real surface? For integral-order beams, the explanation is atomic steps. Atomic steps will be present on nearly all crystalline surfaces. At the very least a step density sufficient to account for any misorientation of the sample from perfectly flat must be included. Diffraction is sensitive to atomic steps.[9] They will show up in the RHEED pattern as streaking or as splitting of the diffracted beam at certain diffraction conditions that depend on the path difference of a wave scattered from atomic planes displaced by an atomic step height. If the path difference is an odd multiple of $\lambda/2$, the waves scattered

from each plane will destructively interfere. For such a diffraction condition (called an out-of-phase condition) the surface will appear to be made up of finite sized patches and the reciprocal lattice rod will be broadened. In contrast, if the path length differs by an integral multiple of λ, the surface will appear perfect to that wave and the no broadening is observed. This is called an in-phase condition. The width of a reciprocal-lattice rod at the out-of-phase condition is proportional to the step density on the surface. Another type of disorder that will broaden superlattice rods only, is the presence of antiphase domains. These domains occur because patches of reconstructed surface can nucleate in positions shifted from one another. Electrons will scatter incoherently from them, each domain acting as if it were a 2D crystal of finite size. This broadening will be independent of the position along the superlattice rod; i.e., there are no in-phase or out-of-phase positions for this kind of disorder.

Transmission features will be present if the surface is sufficiently rough. These arise because electrons with RHEED energies can penetrate on the order of 100 Å through a solid before inelastically scattering. In RHEED, surface sensitivity is obtained in part from the grazing geometry; i.e., electrons must travel a long distance before seeing planes deep in the bulk. For a rough surface, asperities rising above the surface will be struck at a less glancing angle and if the asperity is thin enough in the primary-beam direction, transmission will occur. Transmitted electrons will see the additional periodicity of the atomic planes below the surface. As a result, a constraint on **S** in the direction perpendicular to the surface is added and the reciprocal lattice will be an array of points instead of rods. Because transmission can occur only through thin objects, the 3D reciprocal-lattice points from the asperities will be elongated in the direction of the primary beam. The Ewald sphere will intersect a number of the reciprocal-lattice points in the plane containing the 0th Laue circle (called the 0th Laue zone), giving rise to a pattern that will appear as a regular array of spots. It appears as a projection of the reciprocal lattice plane that is nearly perpendicular to the incident beam. The spacing of the spots is inversely related to the spacing of planes in the crystal.

In addition to differences in their appearances, a practical way to differentiate between transmission and reflection features is by observing the diffraction pattern while changing the incident azimuth. The intensity of transmission features will change as the azimuth is changed, but their location will not. In contrast, reflection features (other than the (0, 0) beam) will move continuously either closer to or farther away from the shadow edge as the azimuth is changed, a result of the intersection of the Ewald sphere with a rod moving up or down as the azimuth is changed.

Film Growth

One of the main uses of RHEED is to monitor crystal structure during film growth in ultrahigh vacuum. Its ability to distinguish between 2D and 3D structure gives

direct evidence on the growth mode of a film. The onset of clustering is associated with the appearance of transmission features. In 2D film growth, changes in the surface lattice periodicity (reconstruction) show up in the appearance or disappearance of superlattice features,[10] while roughness shows up as a change in the shape of the RHEED features. In addition, changes in the separation between RHEED streaks, which relate directly to changes in the surface lattice constant, can be used to follow strain relaxation.

In films that grow 2D for many layers, "intensity oscillations" have been observed for certain growth conditions using RHEED[11] and LEED. Observation is made by monitoring the intensity of a diffracted beam as a function of time during growth. The period of an oscillation corresponds to the time it takes to deposit a monolayer. In practice, oscillations are frequently used to calibrate deposition rates.

Oscillations arise from periodic changes in the surface structure as a deposited layer nucleates, grows, and then fills in the previously deposited layer. They can be understood qualitatively within the framework developed in the discussion of atomic steps. As a material is deposited, 2D islands nucleate, increasing the step density. This causes diffraction features to become smeared out, reducing their intensity at the location of the detector. As the surface becomes covered, the intensity recovers. This process is repeated, with continued deposition causing the intensity to oscillate. Further evidence for this interpretation has been obtained from the analysis of RHEED diffracted-beam profiles for the growth of GaAs on GaAs (100), where the shape of diffracted beams has been modeled to extract step densities.[12]

While kinematic diffraction theory describes intensity oscillations adequately in some cases, there are problems with it when it is used to analyze RHEED measurements. The period of the oscillations is correctly predicted, but not necessarily the phase. In spite of these complications, intensity oscillations are evidence for periodic changes in the surface structure.

For deposited materials that are not perfectly lattice-matched to a substrate, strain will build up in the deposited layer until eventually it becomes energetically favorable for 3D clusters of the deposited material's relaxed crystal structure to form. Some materials will not wet a substrate at all, and grow as 3D clusters at submonolayer coverages. RHEED can give information on cluster orientations, shapes, and sizes. Figure 4a is a photograph of a RHEED pattern obtained for 4 monolayers of In deposited on cleaved GaAs (110). The regular array of spots is clearly a transmission pattern and indicates that the deposited In has formed 3D clusters. The pattern can be indexed with the symmetry and spacing of an Indium [110] reciprocal lattice plane, as shown in Figure 4b. Since all spots are accounted for, clusters present are oriented in the same direction with respect to the substrate. Different orientations would show up as additional arrays of spots, and in the limit of a random orientation the pattern would appear as continuous rings centered about (0,0,0). Information on cluster shape can be extracted if the clusters have a

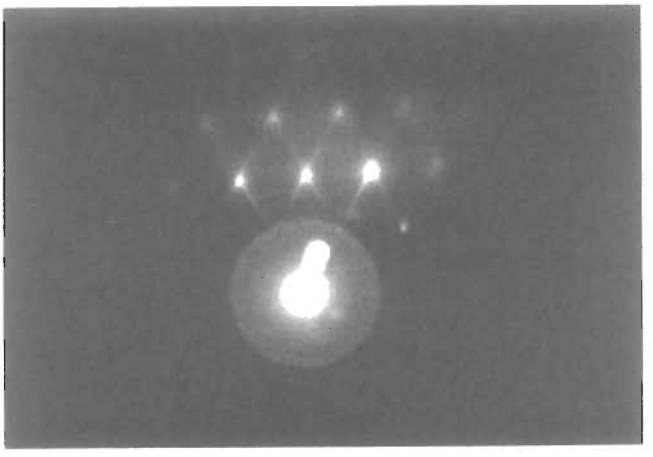

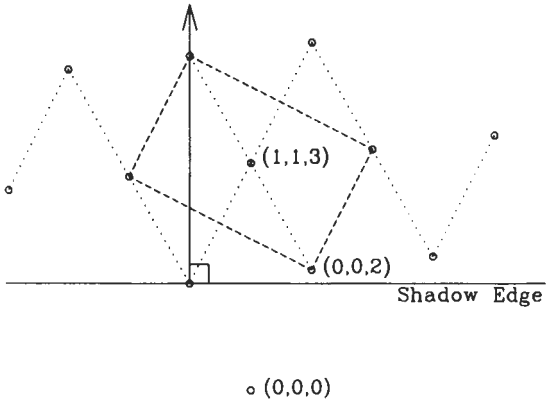

Figure 4 **(a) Photograph of a RHEED pattern for 4 monolayers of In deposited on cleaved GaAs (110). The primary beam is incident along the GaAs [110] azimuth. The regular array of spots are a result of transmission diffraction through indium 3D clusters. The streaks of intensity connecting the spots are from the reflection pattern off facets of the In clusters. (b) Spots in the photo can be indexed as the In [$\bar{1}$10] reciprocal-lattice plane oriented so that the In (113) real-space plane is in contact with the substrate.**

preferred orientation and are bounded by crystal facets. In Figure 5a the streaks connecting the spots are reflection features from In facet planes. (They are from (111)- and (001)-type facets.) Cluster size information is contained in the shape of the transmitted features and attempts have been made to extract quantitative values.[13]

Conclusions

RHEED is a powerful tool for studying the surface structure of crystalline samples in vacuum. Information on the surface symmetry, atomic-row spacing, and evidence of surface roughness are contained in the RHEED pattern. The appearance of the RHEED pattern can be understood qualitatively using simple kinematic scattering theory. When used in concert with MBE, a great deal of information on film growth can be obtained.

The time evolution of the RHEED pattern during film growth or during post-growth annealing is a subject of current interest. RHEED intensity oscillations have been observed to damp out over time during deposition. If growth is interrupted the RHEED pattern recovers. Initial attempts have been made to extract surface diffusion coefficients and activation energies by measuring the rate of such processes at different temperatures.

RHEED intensities cannot be explained using the kinematic theory. Dynamical scattering models of RHEED intensities are being developed.[14] With them one will be able to obtain positions of the surface atoms within the surface unit cell. At this writing, such modeling has been done primarily for LEED.

RHEED differs from LEED because of its grazing geometry and higher electron energies. It is the grazing geometry that allows RHEED to be used in concert with film growth. In addition, both reflected and forward scattered (transmitted) electrons can be observed with RHEED. The latter are not detected with LEED, making it less suited for the study of 3D roughness, i.e., clusters or very rough surfaces.

Related Articles in the Encyclopedia

LEED and XRD

References

1 L. de Broglie. Dissertation, Paris, 1924.

2 C. J. Davisson and L. H. Germer. *Phys. Rev.* **30,** 705, 1927.

3 For a basic treatment of interference and diffraction from a 1D grating, see E. Hecht. *Optics.* Addison-Wesley, Reading, 1987, Chapter 10.

4 For a review on the formulation of kinematic diffraction theory with emphasis on the scattering of low-energy electrons, see M. G. Lagally and M. B. Webb. In: *Solid State Physics.* (H. Ehrenreich, F. Seitz, and D. Turnbull, eds.) Academic, New York, 1973, Volume 28.

5 For more detail on the geometrical relationship between the RHEED pattern and the surface crystal structure, see J. E. Mahan, K. M. Geib, G. Y. Robinson, and R. G. Long. *J. Vac. Sci. Technol.* **A8,** 3692, 1990.

6 For a review of how various surface reconstructions appear in a diffraction pattern, see M. A. Van Hove, W. H. Weinberg, and C. -M. Chan. *Low-Energy Electron Diffraction.* Springer, Berlin, 1986, Chapter 3.

7 S. Hasegawa, H. Daimon, and S. Ino. *Surf. Sci.* **187,** 138, 1987.

8 For a review of how defects manifest themselves in a LEED experiment, see M. Henzler. In: *Electron Spectroscopy for Surface Analysis.* (H. I. Ibach, ed.) Springer, Berlin, 1977.

9 For more information on kinematic treatment of diffraction from stepped surfaces, see M. G. Lagally, D. E. Savage, and M. C. Tringides. In: *Reflection High-Energy Electron Diffraction and Reflection Electron Imaging of Surfaces.* NATO ASI Series B, Plenum, New York, 1988, Volume 188.

10 Surface phase transformations and surface chemical reactions are followed by studying the time evolution of superlattice beams originating from monolayer or submonolayer films. See, for example, Chapters 8–10 in *Low-Energy* Van Hove et al. (*op cit.*).

11 For an overview on RHEED intensity oscillations, see B. A. Joyce, J. H. Neave, J. Zhang, and P. J. Dobson. In: *Reflection* NATO (*op cit.*).

12 P. I. Cohen, P. R. Pukite, J. M. Van Hove, and C. S. Lent. *J. Vac. Sci. Tech nol.* **A4,** 1251, 1986.

13 D. E. Savage and M. G. Lagally. *J. Vac. Sci. Technol.* **B4,** 943, 1986.

14 J. L. Beeby. *Reflection* NATO (*op cit.*).